1,2-Phenylene-Bridged Diporphyrin Linked with Porphyrin Monomer and Pyromellitimide as a Model for a Photosynthetic Reaction Center: Synthesis and Photoinduced Charge Separation

Atsuhiro Osuka,*[1a] Satoshi Nakajima,[1a] Kazuhiro Maruyama,[1a] Noboru Mataga,*[1b] Tsuyoshi Asahi,[1b] Iwao Yamazaki,[1c] Yoshinobu Nishimura,[1c] Takeshi Ohno,[1d] and Koichi Nozaki[1d]

Contribution from the Department of Chemistry, Faculty of Science, Kyoto University, Kyoto 606, Japan, Department of Chemistry, Faculty of Engineering Science, Osaka University, Toyonaka 560, Japan, Department of Chemical Process Engineering, Faculty of Engineering, Hokkaido University, Sapporo 060, Japan, and Department of Chemistry, College of General Education, Osaka University, Toyonaka 560, Japan

Received August 24, 1992

Abstract: The synthesis and excited-state dynamics are described for fixed-distance zinc diporphyrin–zinc porphyrin–pyromellitimide molecules **1–3** (D–M–Im) and zinc porphyrin–pyromellitimide molecule **7** (M–Im). In molecules **1–3**, D and M–Im moieties are bridged by aromatic spacers such as 4,4′-biphenylylene-, 1,4-phenylene-, and methylenebis-(1,4-phenylene) groups, respectively. The rates of charge separation (CS) and charge recombination (CR), k_{CS} and k_{CR}, of **7** were determined in C_6H_6, THF, and DMF. k_{CS} in **7** is essentially solvent polarity independent, while k_{CR} increases with solvent polarity. A small k_{CR} in C_6H_6 has been interpreted in terms of the small electron-transfer probability, which arises from the small solvent reorganization energy and large reaction exothermicity in the inverted region. In molecules **1–3**, ^{1}(M)* is competitively quenched by D through the intramolecular singlet–singlet energy transfer to give ^{1}(D)*–M–Im and by Im through intramolecular CS to give D–$(M)^+$–$(Im)^-$. The ^{1}(D)*–M–Im state decays to the ground state with a lifetime to that of the reference ^{1}(D)* and does not undergo any intramolecular electron-transfer reactions. On the other hand, from the initially formed ion pair (IP) state, D–$(M)^+$–$(Im)^-$, a secondary IP state, $(D)^+$–M–$(Im)^-$, is formed by hole transfer from $(M)^+$ to D in THF or DMF. Such hole transfer does not occur in less polar C_6H_6. The lifetimes of the secondary IP states formed from **1**, **2**, and **3**, which range from 0.25 to 23 μs, depend upon both the spacer connecting the D and M and the polarity of solvent. In contrast to the case of $(M)^+$–$(Im)^-$, the lifetime of $(D)^+$–M–$(Im)^-$ increases with increasing solvent polarity. Marked differences in solvent polarity effects observed on the lifetime of the $(M)^+$–$(Im)^-$ and $(D)^+$–M–$(Im)^-$ states may have important practical implications for the design of artificial photosynthetic models.

Introduction

The appearance[2-4] of the X-ray structure of a bacterial photosynthetic reaction center (RC) has exerted a great impact on mechanistic[5-7] as well as synthetic approaches toward this natural charge-separation (CS) apparatus.[8-12] In the RC, six tetrapyrrolic subunits and two quinones are positioned at precise distances and orientations to realize a rapid energy relay with the special pair (SP) as the final energy sink and a highly efficient CS with the SP as the initial electron donor. In fact, irradiation of either bacteriochlorophyll (BChl) or bacteriopheophytin (BPh) in the RC leads to the instantaneous population of ^{1}(SP)* in less than 150 fs, from which a stable ion pair (IP) state, $(SP)^+$–BChl–$(BPh)^-$, is formed within ca. 3 ps; its charge-recombination (CR) rate is less than 10^8 s^{-1}.[13] A subsequent electron transfer (ET) from $(BPh)^-$ to Q_A occurs in ca. 200 ps to yield $(SP)^+$–BChl–BPh–$(Q_A)^-$ which, in the absence of Q_B, survives for about 100 ms before a CR reaction occurs. More recent reports suggest the involvement of an $(SP)^+$–$(BChl)^-$ state as a discrete chemical intermediate in the initial CR process.[14] In order to better understand the detailed mechanism in the RC, it would be desirable to develop covalently linked molecular

(1) (a) Kyoto University. (b) Faculty of Engineering Science, Osaka University. (c) Hokkaido University. (d) College of General Education, Osaka University.

(2) (a) Deisenhofer, J.; Epp, O.; Miki, K.; Huber, R.; Michel, H. *J. Biol. Chem.* **1984**, *180*, 385. (b) Deisenhofer, J.; Epp, O.; Miki, K.; Huber, R.; Michel, H. *Nature* **1985**, *318*, 618. (c) Michel, H.; Epp, O.; Deisenhofer, J. *EMBO J.* **1986**, *5*, 2445.

(3) (a) Chang, C.-H.; Tiede, D. M.; Tang, J.; Smith, U.; Norris, J. R.; Schiffer, M. *J. Mol. Biol.* **1985**, *186*, 201. (b) Chang, C.-H.; Tiede, D. M.; Tang, J.; Norris, J. R.; Schiffer, M. *FEBS Lett.* **1986**, *205*, 82.

(4) (a) Allen, J. P.; Feher, G.; Yeates, T. O.; Komiya, H.; Rees, D. C. *Proc. Natl. Acad. Sci. U.S.A.* **1987**, *84*, 5730. (b) Allen, J. P.; Feher, G.; Yeates, T. O.; Komiya, H.; Rees, D. C. *Ibid.* **1987**, *84*, 6162. (c) Yeates, T. O.; Komiya, H.; Chirino, A.; Rees, D. C.; Allen, J. P.; Feher, G. *Ibid.* **1988**, *85*, 7993. (d) Allen, J. P.; Feher, G.; Yeates, T. O.; Komiya, H.; Rees, D. C. *Ibid.* **1988**, *85*, 8487.

(5) DeVault, D. *Quantum-Mechanical Tunneling in Biological Systems*; Cambridge University Press: Cambridge, U.K., 1984.

(6) Friesner, R. A.; Won, Y. *Biochim. Biophys. Acta* **1989**, *977*, 99.

(7) (a) Bixon, M.; Jortner, J.; Michel-Beyerle, M. E.; Ogrodnik, A. *Biochim. Biophys. Acta* **1989**, *977*, 273. (b) Bixon, M.; Jortner, J.; Michel-Beyerle, M. E. *Ibid.* **1991**, *1056*, 301. (c) Chan, C.-K.; DiMagno, T. J.; Chen, L. X.-Q.; Norris, J. R.; Fleming, G. R. *Proc. Natl. Acad. Sci. U.S.A.* **1991**, *88*, 11202.

(8) Boxer, S. G. *Biochim. Biophys. Acta* **1983**, *726*, 265.

(9) Connolly, J.; Bolton, J. R. In *Photoinduced Electron Transfer*, Part D; Fox, M. A., Chanon, M., Eds.; Elsevier: Amsterdam, 1988; p 303.

(10) (a) Wasielewski, M. R. *Photochem. Photobiol.* **1988**, *47*, 923. (b) Wasielewski, M. R. In *Photoinduced Electron Transfer*, Part A; Fox, M. A., Chanon, M., Eds.; Elsevier: Amsterdam, 1988; p 161. (c) Wasielewski, M. R. *Chem. Rev.* **1992**, *92*, 435.

(11) Gust, D.; Moore, T. A. *Science* **1989**, *244*, 35.

(12) Maruyama, K.; Osuka, A. *Pure Appl. Chem.* **1990**, *62*, 1511.

(13) (a) Parson, W. W. *New Comprehensive Biochemistry: Photosynthesis*; Amesz, J., Ed.; **1987**, 43. (b) Kirmaier, C.; Holten, D. *Photosyn. Res.* **1987**, *13*, 225. (c) Martin, J.-L.; Breton, J.; Hoff, A. J.; Migus, A.; Antonetti, A. *Proc. Natl. Acad. Sci. U.S.A.* **1986**, *83*, 957. (d) Breton, J.; Martin, J.-L.; Migus, A.; Antonetti, A.; Orszag, A. *Ibid.* **1986**, *83*, 5121. (e) Wasielewski, M. R.; Tiede, D. M. *FEBS Lett.* **1986**, *204*, 368. (f) Kirmaier, C.; Holten, D. *FEBS Lett.* **1988**, *239*, 211. (g) Kirmaier, C.; Holten, D. *Proc. Natl. Acad. Sci. U.S.A.* **1990**, *87*, 3552. (h) Vos, M. H.; Lambry, J.-C.; Robles, S.; Youvan, D. C.; Breton, J.; Martin, J.-L. *Ibid.* **1991**, *88*, 8885. (i) Vos, M. H.; Lambry, J.-C.; Robles, S.; Youvan, D. C.; Breton, J.; Martin, J.-L. *Ibid.* **1992**, *89*, 613.

0002-7863/93/1515-4577$04.00/0

assemblies that provide a closer mimic of complicated chromophore compositions and three-dimensional arrangements of such photosynthetic pigments and to investigate their fast photoexcited kinetics by ultrafast laser photolysis techniques. However, the unequivocal identification and absolute measurement of short-lived radical-ion species by their optical absorption is often quite difficult in porphyrin–quinone molecules, since the absorption spectra of porphyrin cation radicals are quite similar to those of porphyrin S_1 or T_1 states and the spectral characteristics of quinone anion radicals are rather obscure. Thus, in most cases, only the rates of CS between the singlet excited state of porphyrin and quinone have been determined from the diminished fluorescence lifetime of the porphyrin.[15] Direct detection of IP states formed from porphyrin–quinone molecules by transient absorption spectroscopy has been rather limited.[16,17]

Generation of a long-lived IP state via initial ET within the singlet manifold is apparently an important issue in the field of model studies. In recent years, multistep electron-transfer strategies based on multicomponent donor–acceptor systems have been successfully employed to realize long-lived IP states.[17,18] In order to realize a long-lived IP state with high quantum yields as observed in the natural photosynthetic reaction center, it is highly desirable to elucidate factors that control the quantum yields and lifetimes of multicomponent IP states. Gust and Moore[11,19] have extensively explored the use of carotenoids as secondary electron donors to promote long-lived charge separation in supramolecular systems. One of the advantages of their model is the characteristic strong absorption of the carotenoid cation radical, which is observed around 980 nm in CH_2Cl_2 and by which one can clearly monitor the electron transfer from the carotenoid subunit to the porphyrin cation radical generated in the ET reaction with the linked quinone. With these advantages in hand, Gust and Moore have developed many carotenoid–porphyrin–quinone molecules in which multistep electron transfer indeed results in a long-lived IP state.[11,19] Conformationally restricted, fixed-distance porphyrin models bearing both amine electron-donor and quinone electron-acceptor groups have been shown to be quite effective in realizing long-lived IP states even at 5 K.[20b] However, we are not aware of any in which a porphyrin dimer donates an electron to a porphyrin monomer to effect a long-lived IP state as observed in the natural RC. We are also not aware of models realizing unidirectional, intramolecular singlet–singlet energy transfer from monomeric porphyrin to a diporphyrin chromophore. Recently, we have prepared conformationally restricted trimeric and tetrameric porphyrin models in which a 1,8-anthracene-pillared zinc porphyrin dimer and quinone are connected across one or two zinc porphyrins.[21] Although formation of a long-lived IP state with a lifetime of ca. several nanoseconds was detected by transient absorption spectroscopy, the quantum yield was very small.[22]

We report here the synthesis and excited-state dynamics of triad molecules **1–3**, in which the diporphyrin unit (D) is connected with a monomeric porphyrin (M) and a pyromellitimide acceptor (Im).[23] Our design of **1–3** is based on the following characteristic features of the respective components: firstly, the 1,2-phenylene-bridged zinc diporphyrin shows significantly stronger electronic interactions that result in both the reduction of the one-electron oxidation potential and the lowering of the energy level of the S_1 state.[24] X-ray analysis of the reference compound **9** has revealed that the two porphyrin rings take on a nearly parallel conformation with an average interplanar distance of 3.45 Å, a dihedral angle of 6.6°, and a slipped offset conformation with a rotation angle of 22.7°.[24] On the other hand, the ^{1}H-NMR spectrum of **9** in $CDCl_3$ contains only half the number of signals predicted by the crystal structure, indicating a very rapid interconversion between the two enantiomeric conformers in solution. The strong interactions between the two porphyrins in D results in the lowering of the S_1 excitation energy by 0.16 eV in C_6H_6 and THF, and 0.23 eV in DMF, and also in the decrease of the one-electron oxidation potential by 0.24 V in DMF. These properties, which may be directly compared to those of the special pair in RC, make the D moiety a promising excitation-energy acceptor from M and a potential electron donor to $(M)^+$ in models **1–3** (Chart I).

Secondly, the pyromellitimide moiety (Im) is an effective electron acceptor toward the singlet excited state of M and has been proven to be quite useful for analysis of ET kinetics because of the characteristic sharp absorption at ca. 715 nm due to $(Im)^-$.[23,25,26] The pyromellitimide unit was used earlier by Sanders et al. as an electron acceptor toward the singlet excited state of

(14) (a) Holtzapfel, W.; Finkele, U.; Kaiser, W.; Oesterhelt, D.; Scheer, H.; Stilz, H. U.; Zinth, W. *Chem. Phys. Lett.* **1989**, *160*, 1. (b) Holtzapfel, W.; Finkele, U.; Kaiser, W.; Oesterhelt, D.; Scheer, H.; Stilz, H. U.; Zinth, W. *Proc. Natl. Acad. Sci. U.S.A.* **1990**, *87*, 5168. (c) Lauterwasser, C.; Finkele, U.; Scheer, H.; Zinth, W. *Chem. Phys. Lett.* **1991**, *183*, 471. (d) Dressler, K.; Umlauf, E.; Schmidt, S.; Hamm, P.; Zinth, W.; Buchanan, S.; Michel, H. *Chem. Phys. Lett.* **1991**, *183*, 270.

(15) For reviews of this area, see: refs **9** and 10c. For recent papers, see: Osuka, A.; Tomita, H.; Maruyama, K. *Chem. Lett.* **1988**, 1205. Sakata, Y.; Nakashima, Y.; Goto, Y.; Tatemitu, H.; Misumi, S.; Asahi, T.; Hagihara, M.; Nishikawa, S.; Okada, T.; Mataga, N. *J. Am. Chem. Soc.* **1989**, *111*, 8970. Sakata, Y.; Tsue, H.; Goto, Y.; Misumi, S.; Asahi, T.; Nishikawa, S.; Okada, T.; Mataga, N. *Chem. Lett.* **1991**, 1307. Heitele, H.; Pollinger, F.; Kremer, K.; Michel-Beyerle, M. E.; Voir, F. G.; Weiser, J.; Staab, H. A. *Chem. Phys. Lett.* **1992**, *188*, 270. Rempel, U.; Maltan, B. V.; Borczyskowski, C. V. *Chem. Phys. Lett.* **1990**, *169*, 347. Gersdorff, J. V.; Huber, M.; Schubert, H.; Niethammer, D.; Kirste, B.; Plato, M.; Möbius, K.; Kurreck, H.; Eichberger, R.; Kietzmann, R.; Willig, F. *Angew. Chem., Int. Ed. Engl.* **1990**, *29*, 670. Kamioka, K.; Cormier, R. A.; Lutton, T. A.; Connolly, J. S. *J. Am. Chem. Soc.* **1992**, *114*, 4414. See, also: ref 53.

(16) (a) Migita, M.; Okada, T.; Mataga, N.; Nishitani, S.; Kurata, N.; Sakata, Y.; Misumi, S. *Chem. Phys. Lett.* **1981**, *84*, 263. (b) Nishitani, S.; Kurata, N.; Sakata, Y.; Misumi, S.; Karen, A.; Okada, T.; Mataga, N. *J. Am. Chem. Soc.* **1983**, *105*, 7771. (c) Mataga, N.; Karen, A.; Okada, T.; Nishitani, S.; Kurata, N.; Sakata, Y.; Misumi, M. *J. Phys. Chem.* **1984**, *88*, 5138. (d) Wasielewski, M. R.; Niemczyk, M. P. *J. Am. Chem. Soc.* **1984**, *106*, 5043. Wasieleweski, M. R.; Niemczyk, M. P.; Svec, W. A.; Pewitt, E. B. *J. Am. Chem. Soc.* **1985**, *107*, 1080. (e) Knapp, S.; Murali Dhar, T. G.; Albaneze, J.; Gentemann, S.; Potenza, J. A.; Holten, D.; Schugar, H. J. *J. Am. Chem. Soc.* **1991**, *113*, 4010. (f) Frey, W.; Klann, R.; Elsaesser, T.; Baumann, E.; Futscher, M.; Staab, H. A. *Chem. Phys. Lett.* **1992**, *190*, 567. (g) Hamanoue, K.; Nakayama, T.; Nanshow, H.; Ushida, K.; Naruta, Y.; Kodo, T.; Maruyama, K. *Chem. Phys. Lett.* **1991**, *187*, 409. See, also: refs 20, 22, 35, 38b, and 60d.

(17) Mataga, N. *Pure Appl.* Chem. **1984**, *56*, 1255.

(18) For the first example, see: ref 16b. See also: refs 19, 20, and 60.

(19) (a) Moore, T. A.; Gust, D.; Mathis, P.; Mialocq, J.-C.; Chachaty, C.; Bensasson, R. V.; Land, E. J.; Doizi, D.; Liddell, P. A.; Lehman, W. R.; Nemeth, G. A.; Moore, A. L. *Nature* **1984**, *307*, 630. (b) Seta, P.; Bienvenue, E.; Moore, A. L.; Mathis, P.; Bensasson, R. V.; Liddell, P.; Pessiki, P. J.; Joy, A.; Moore, T. A.; Gust, D. *Nature* **1985**, *316*, 653. (c) Liddell, P. A.; Barrett, D.; Makings, L. R.; Pessiki, P. J.; Gust, D.; Moore, T. A. *J. Am. Chem. Soc.* **1986**, *108*, 5350. (d) Gust, D.; Moore, T. A.; Makings, L. R.; Liddell, P. A.; Nemeth, G. A.; Moore, A. L. *J. Am. Chem. Soc.* **1986**, *108*, 8023. (e) Gust, D.; Moore, T. A.; Liddell, P. A.; Nemeth, G. A.; Makings, L. R.; Moore, A. L.; Barrett, D.; Pessiki, P. J.; Bensasson, R. V.; Rougée, M.; Chachaty, C.; De Schryver, F. C.; van der Auweraer, M.; Holzwarth, A. R.; Connolly, J. S. *J. Am. Chem. Soc.* **1987**, *109*, 846. (f) Gust, D.; Moore, T. A.; Moore, A. L.; Barrett, D.; Harding, L. O.; Makings, L. R.; Liddell, P. A.; De Schryver, F. C.; van der Auweraer, M.; Bensasson, R.; Rougée, M. *J. Am. Chem. Soc.* **1988**, *110*, 321. (g) Gust, D.; Moore, T. A.; Moore, A. L.; Makings, L. R.; Seely, G. R.; Ma, X.; Trier, T. T.; Gao, F. *J. Am. Chem. Soc.* **1988**, *110*, 7567. (h) Gust, D.; Moore, T. A.; Moore, A. L.; Seely, G.; Liddell, P.; Barrett, D.; Harding, L. O.; Ma, X. C.; Lee, S.-J.; Gao, F. *Tetrahedron* **1989**, *45*, 4867. (i) Gust, D.; Moore, T. A.; Moore, A. L.; Lee, S.-J.; Bittersmann, E.; Luttrull, D. K.; Rehms, A. A.; DeGraziano, J. M.; Ma, X. C.; Gao, F.; Belford, R. E.; Trier, T. T. *Science* **1990**, *248*, 199. (j) Hasharoni, K.; Levanon, H.; Tang, J.; Bowman, M. K.; Norris, J. R.; Gust, D.; Moore, T. A.; Moore, A. L. *J. Am. Chem. Soc.* **1990**, *112*, 6477.

(20) (a) Wasielewski, M. R.; Niemczyk, M. P.; Svec, W. A.; Pewitt, E. B. *J. Am. Chem. Soc.* **1985**, *107*, 5562. (b) Wasielewski, M. R.; Gaines, G. L., III; O'Neil, M. P.; Svec, W. A.; Niemczyk, M. P. *J. Am. Chem. Soc.* **1990**, *112*, 4559.

(21) Osuka, A.; Nagata, T.; Maruyama, K. *Chem. Lett.* **1991**, 481.

(22) Osuka, A.; Maruyama, K.; Mataga, N.; Asahi, T.; Yamazaki, I.; Tamai, N.; Nishimura, Y. *Chem. Phys. Lett.* **1991**, *181*, 413.

(23) For a preliminary report of this work, see: Osuka, A.; Nakajima, S.; Maruyama, K.; Mataga, N.; Asahi, T. *Chem. Lett.* **1991**, 1003.

(24) Osuka, A.; Nakajima, S.; Nagata, T.; Maruyama, K.; Toriumi, K. *Angew. Chem., Int. Ed. Engl.* **1991**, *30*, 582.

(25) Osuka, A.; Nagata, T.; Maruyama, K.; Mataga, N.; Asahi, T.; Yamazaki, I.; Nishimura, Y. *Chem. Phys. Lett.* **1991**, *185*, 88.

(26) Osuka, A.; Yamada, H.; Maruyama, K.; Mataga, N.; Asahi, T.; Yamazaki, I.; Nishimura, Y. *Chem. Phys. Lett.* **1991**, *181*, 419.

Chart I. Structures of the Models Studied in this Paper

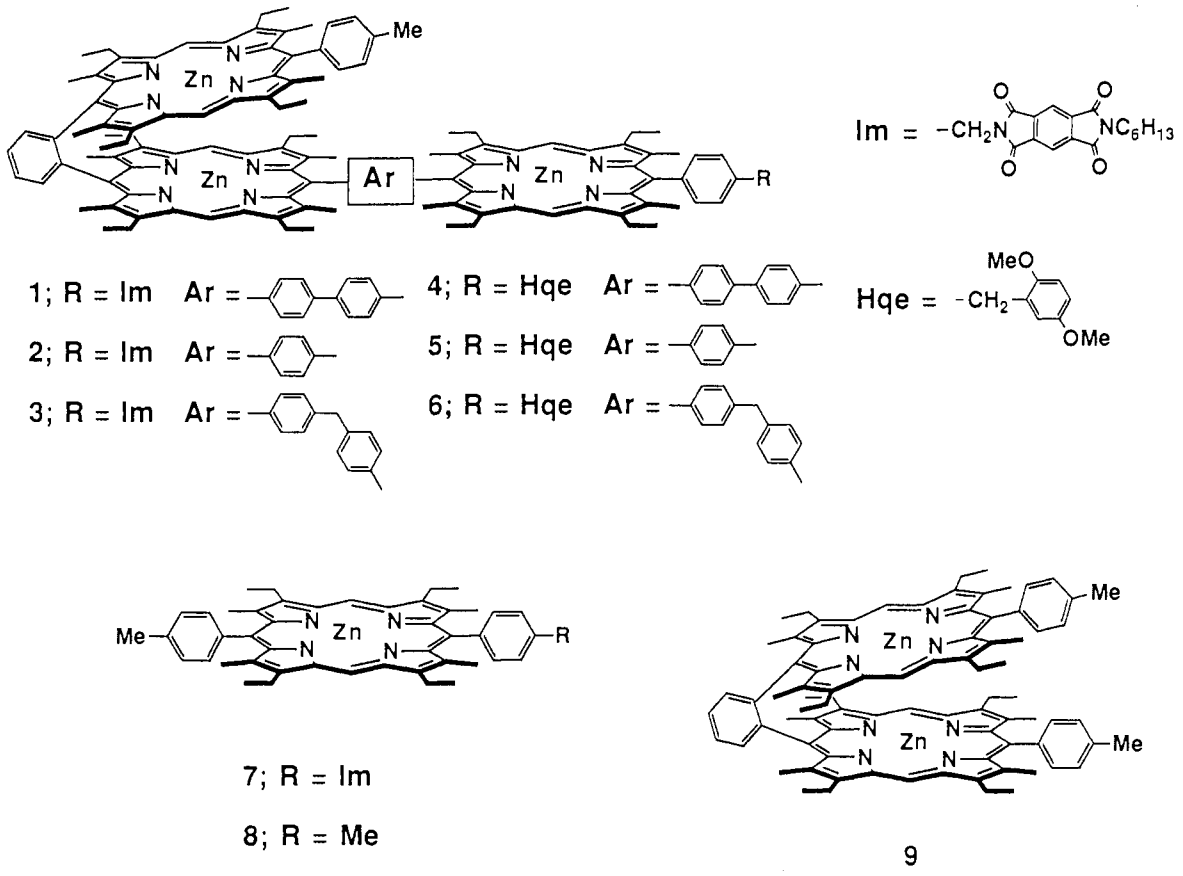

porphyrins.[27-29] These workers prepared a wide variety of model compounds such as pyromellitimide-capped porphyrins, pyromellitimide-capped porphyrin dimers, and pyromellitimide-bridged cyclic porphyrin dimers. They have also conducted picosecond time-resolved absorption spectroscopy on the pyromellitimide-capped porphyrins in solvents having a wide range of dielectric constants. However, they monitored the transient absorption spectra only in a narrow range of 420–540 nm and thus missed observing the characteristic absorption of $(Im)^{-}$.[29]

In the reference diporphyrin-free monomeric model **7** (M–Im), the center-to-center distance between M and Im is restricted to be ca. 13 Å (estimated from Corey–Pauling–Koltun models). In **1–3**, D is connected with the M–Im unit by 4,4′-biphenylylene-, 1,4-phenylene-, and methylenebis(1,4-phenylene) linkages, respectively, and thus the center-to-center distance between D and M may be considered to be restricted to ca. 17.9 Å for **1**, 13.5 Å for **2**, and 15–16.6 Å for **3**, respectively.

Results

Excited-State Dynamics. Absorption and Fluorescence Spectra of Models. In Figure 1, the absorption spectra of **1** and **2** in THF are shown together with those of **7** and **9**. The absorption spectrum of **7** exhibits Q-bands at 505, 538, and 572 nm while that of **9** shows rather broadened Q-bands at 545 (shoulder), 560, and 612 nm. The absorption spectra of **1–3** and **7** are identical to the corresponding acceptor-free compounds **4–6** and **8**, respectively, indicating that attachment of the pyromellitimide moiety to the porphyrin chromophores does not significantly perturb the electronic structure of the porphyrins. The absorption spectrum of **1**, which is virtually the same as that of **3**, is a simple sum of the absorption spectra of **7** and **9**. On the other hand, exciton coupling between D and M results in broadening and red-shifting of the Q-bands in the spectrum of **2**. Later we shall describe the results of laser flash photolysis experiments on **1** by exciting at either 532 or 620 nm. Irradiation at 532 nm leads to population of $^1(D)^*$–M–Im and D–$^1(M)^*$–Im simultaneously, while excitation at 620 nm results in selective population of $^1(D)^*$–M–Im.

Figure 2 shows the fluorescence spectra of **1**, **4**, **8**, and **9** in THF for excitation at 545 nm. The monomeric zinc complex **8** has maxima at 584 and 642 nm; the characteristic vibrational structure of zinc porphyrin is no longer observed in the fluorescence spectrum of **9**, in which the emission maximum is at 660 nm. The fluorescence quantum yield of **9** is ca. 0.12 relative to that of **8**. The reduced fluorescence quantum yield of **9** indicates the presence of additional nonradiative decay channels in $^1(D)^*$. The fluorescence of **9** is not significantly affected by the solvent polarity in a wide range (from C_6H_6 to CH_3CN), suggesting that a solvent-induced intradimer CS does not take place in the S_1 state of **9**. In contrast to the absorption spectra, the steady-state fluorescence spectra of **1** and **4** in THF are quite different from the superposition of the emission spectra of the individual chromophores. In the emission spectra of **1** and **4**, the ratio of the fluorescence intensity of M to that of D is lower, indicating the occurrence of efficient intramolecular singlet–singlet energy transfer (EN) from M to D. The fluorescence from M is more reduced in **1** than in **4** due to an additional intramolecular CS pathway between $^1(M)^*$ and Im.

Photoinduced Electron Transfer in 7. Figure 3b shows the picosecond time-resolved transient absorption spectra of **7** in THF taken by excitation with 532-nm laser pulses. As the $S_n \leftarrow S_1$

(27) (a) Cowan, J. A.; Sanders, J. K. M. *J. Chem. Soc., Perkin Trans. I* **1985**, 2435. (b) Cowan, J. A.; Sanders, J. K. M.; Beddard, G. S.; Harrison, R. J. *J. Chem. Soc., Chem. Commun.* **1987**, 55. (c) Hunter, C. A.; Meah, M. N.; Sanders, J. K. M. *J. Chem. Soc., Chem. Commun.* **1988**, 692–694 and 694. (d) Anderson, H. L.; Hunter, C. A.; Sanders, J. K. M. *J. Chem. Soc., Chem. Commun.* **1989**, 226. (e) Hunter, C. A.; Sanders, J. K. M.; Beddard, G. S.; Evans, S. *J. Chem. Soc., Chem. Commun.* **1989**, 1765.

(28) (a) Hunter, C. A.; Meah, M. N.; Sanders, J. K. M. *J. Am. Chem. Soc.* **1990**, *112*, 5773. (b) Anderson, H. L.; Hunter, C. A.; Meah, M. N.; Sanders, J. K. M. *J. Am. Chem. Soc.* **1990**, *112*, 5780.

(29) Harrison, R. J.; Peace, B.; Beddard, G. S.; Cowan, J. A.; Sanders, J. K. M. *Chem. Phys.* **1987**, *116*, 429.

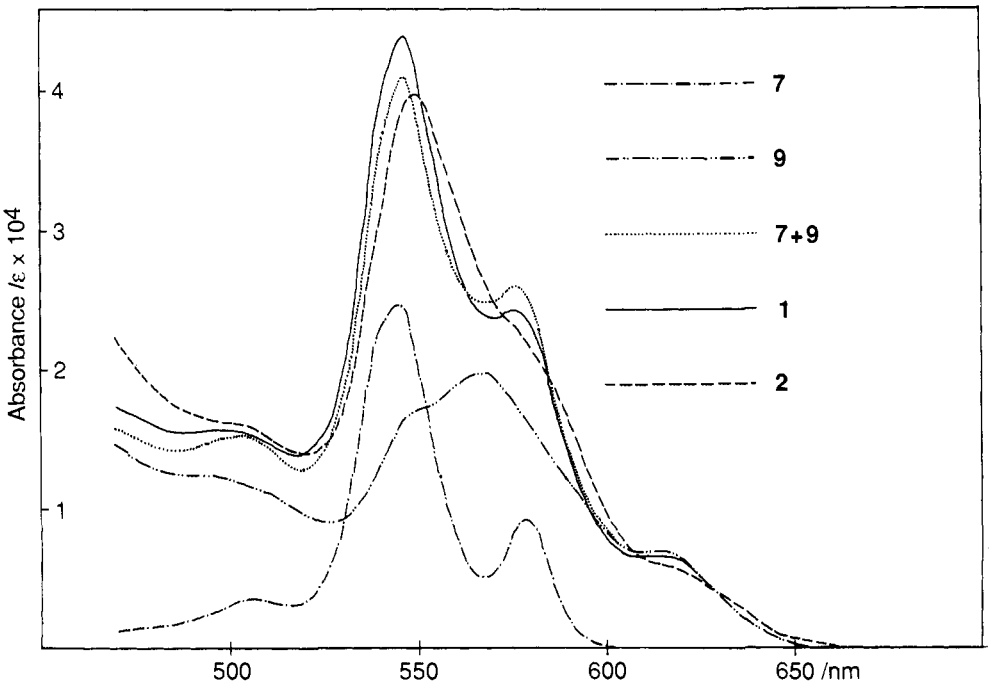

Figure 1. Absorption spectra of **1**, **2**, **7**, and **9** in THF.

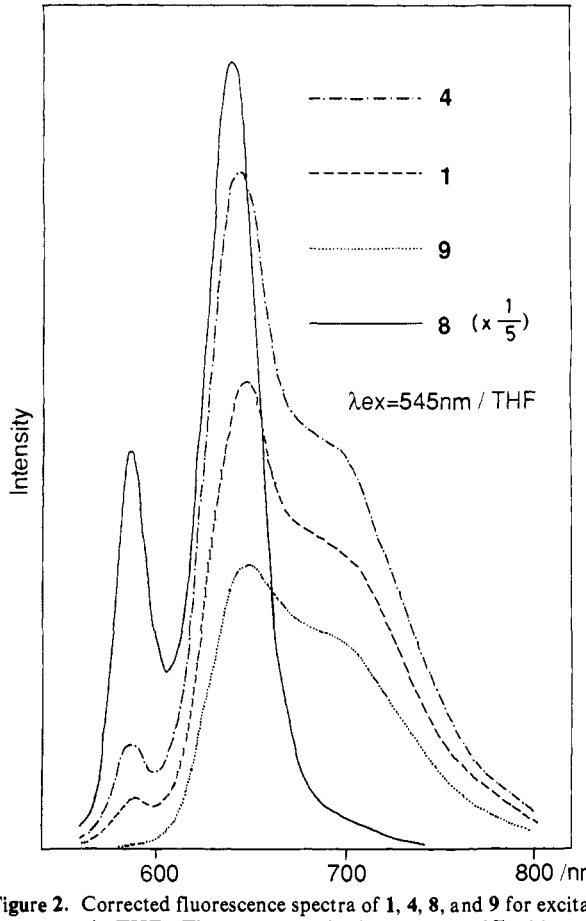

Figure 2. Corrected fluorescence spectra of **1**, **4**, **8**, and **9** for excitation at 545 nm in THF. The spectrum of **8** is shown at 20% of its actual intensity.

absorption band of M at 460 nm decays with τ = 60 ps, a sharp absorption band at 715 nm appears with a rise time of 60 ps and decays with τ = 100 ps. A broad absorption band around 670 nm exhibits the same time profile as that of the 715-nm band. By referring to the spectra obtained by electrochemical oxidation or reduction of the relevant chromophores, the absorption bands at 670 and 715 nm are assigned to $(M)^+$ and $(Im)^-$, respectively. Residual absorption around 460 nm at 1-ns delay time can be assigned from its shape to $^3(M)^*$, which is produced by intersystem crossing competing with CS between $^1(M)^*$ and Im. In the time region of up to several hundreds picoseconds, CS between $^3(M)^*$ and Im can be neglected. Figures 3a and 3c show the transient absorption spectra of **7** in C_6H_6 and DMF, respectively. A large solvent effect on the intramolecular ET reactions in **7** is remarkable in that the absorptions due to the $(M)^+$–$(Im)^-$ IP state are clearly evident even at 3–5-ns delay time in less polar C_6H_6 but are virtually undetectable in the time range of >10 ps to several ns in polar DMF solution.

The results in Figure 3 are depicted by Scheme II, from which the time-dependent concentrations of the $S_1[^1(M)^*–Im]$, $IP[(M)^+–(Im)^-]$, and $T_1[^3(M)^*–Im]$ states are given by the following equations:[35]

$$[S_1] = A_0 \exp(-t/\tau_S)$$

$$[IP] = \{A_0\Phi_{ET}\tau_S^{-1}/(\tau_S^{-1} - \tau_{IP}^{-1})\}\{\exp(-t/\tau_{IP}) - \exp(-t/\tau_S)\}$$

$$[T_1] = A_0(1-\Phi_{ET})\Phi_T\{1-\exp(-t/\tau_S)\}$$

where A_0 is the initial concentration of S_1, $\tau_S^{-1} = k_{CS} + \tau_0^{-1}$, $\tau_0^{-1} = k_F + k_d^1 + k_{ISC}$, $\tau_{IP}^{-1} = k_{CR}$, $\Phi_{ET} = k_{CS}\tau_S$, and $\Phi_T = k_{ISC}\tau_S$. For interpretation of the time-resolved spectra in Figure 3, it is not necessary to take into account the decay of the T_1 state k_d^3, which occurs on a much slower time scale. The time profile of the transient absorbance $A_\lambda(t)$ at wavelength λ is obtained by using the difference absorption coefficients of the S_1 (ϵ_{S_1}), the IP (ϵ_{IP}), and the T_1 (ϵ_{T_1}) states at that wavelength as follows:[35]

(30) Nagata, T.; Osuka, A.; Maruyama, K. *J. Am. Chem. Soc.* **1990**, *112*, 3054.
(31) Clezy, P. S.; Nichol, A. W. *Aust. J. Chem.* **1965**, *11*, 1835.
(32) Lindsey, J. S.; Schreiman, I. C.; Hsu, H. C.; Kearney, P. C.; Marguerettaz, A. M. *J. Org. Chem.* **1987**, *52*, 827. Nagata, T. *Bull. Chem. Soc. Jpn.* **1991**, *64*, 3005.
(33) Osuka, A.; Nagata, T.; Kobayashi, F.; Maruyama, K. *J. Heterocycl. Chem.* **1990**, *27*, 1657.
(34) Weller, A. *Z. Phys. Chem. (N.Y.)* **1982**, *133*, 93.
(35) Asahi, T.; Ohkohchi, M.; Matsusaka, R.; Mataga, N.; Zhang, R. P.; Osuka, A.; Maruyama, K. *J. Am. Chem. Soc.* In press.

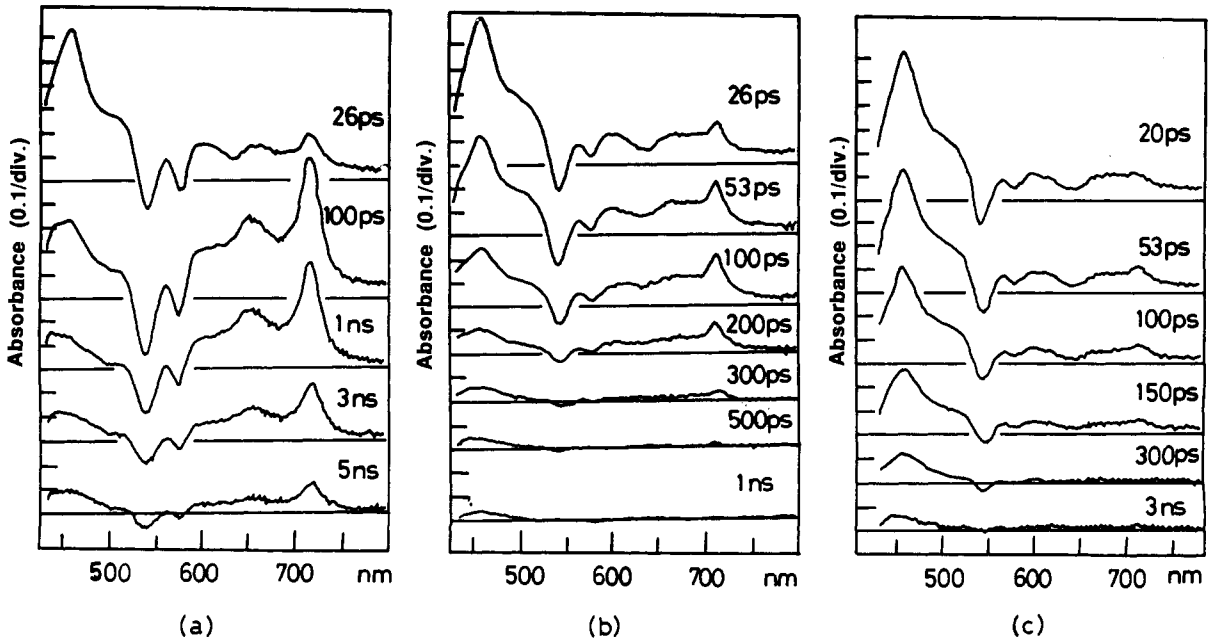

Figure 3. Transient absorption spectra of **7** for excitation at 532 nm in (a) C_6H_6, (b) THF, and (c) DMF.

Scheme I. Synthetic Routes to the Triads **1–6**

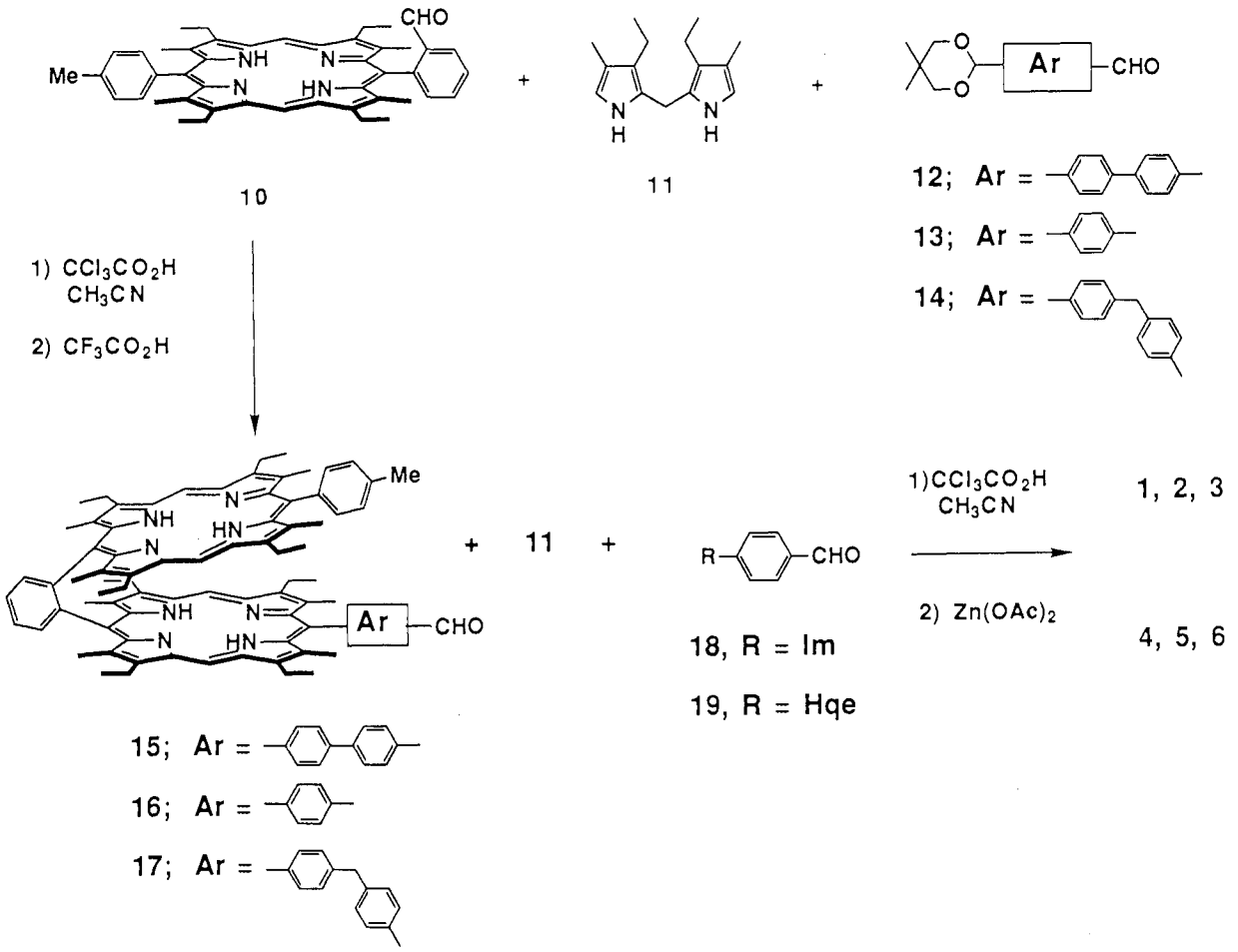

$$A_\lambda(t) = \epsilon_{S_1}[S_1] + \epsilon_{IP}[IP] + \epsilon_{T_1}[T_1]$$
$$= \alpha \exp(-t/\tau_S) + \beta \exp(-t/\tau_{IP}) + \gamma \quad (1)$$

where $\alpha = A_0\{\epsilon_{S_1} - \epsilon_{IP}\Phi_{ET}\tau_S^{-1}/(\tau_S^{-1} - \tau_{IP}^{-1}) - \epsilon_{T_1}(1 - \Phi_{ET})\Phi_T\}$, $\beta = A_0\epsilon_{IP}\Phi_{ET}\tau_S^{-1}/(\tau_S^{-1} - \tau_{IP}^{-1})$, and $\gamma = A_0\epsilon_{T_1}(1-\Phi_{ET})\Phi_T$.

By simulation of the observed time profiles at 460 and 715 nm (720 nm in C_6H_6) (Figure 4) with eq 1, k_{CS} and k_{CR} values have been obtained (Table I). Fluorescence lifetimes of **7** (72 ps in THF, 65 ps in C_6H_6, and 108 ps in DMF)[36] and **8** (1.35 ns in THF, 1.27 ns in C_6H_6, and 1.43 ns in DMF) were also used to

(36) The fluorescence-decay curve of **7** has been analyzed by two exponential equations; 72 ps (99.9%) and 1430 ps (0.1%) in THF, 65 ps (99.8%) and 1500 ps (0.2%) in C_6H_6, and 108 ps (99.4%) and 1360 ps (0.6%) in DMF, respectively. In all three cases, the relative amplitudes of the short-lived component are more than 99%. We adapted these lifetimes as τ(M) in the calculation of k_{CS}.

Scheme II. Reaction Scheme and Energy Diagram for **7** in THF

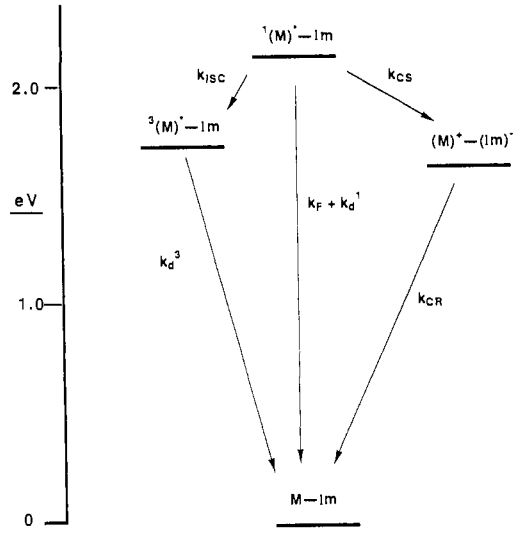

calculate k_{CS} values (Table I), which are in agreement with the rates determined on the basis of the transient absorption data.

Photoexcited Dynamics of 9 and Intramolecular Energy Transfer in 4–6 in THF. Fluorescence decay of **9** could not be satisfactorily reproduced by a single-exponential function (τ = 880 ps (χ^2 = 2.88)), while a biexponential fit gave a reasonably good agreement with τ_1 = 910 ps (84%) and τ_2 = 260 ps (16%) (χ^2 = 1.19). This fluorescence-decay behavior of **9** remains to be fully explored but may be interpreted in terms of changes of the relative geometry of the porphyrins in the relaxation of ^{1}(**9**)*, provided that the most stable conformation in the lowest excited singlet state differs from that in its ground state. The transient absorption spectra of **9** in THF are shown in Figure 5. These spectral changes are interpreted in terms of the population of ^{1}(**9**)* upon photoexcitation followed by intersystem crossing to ^{3}(**9**)*.[37] Analysis of the kinetic trace of the transient absorbance at 643 nm reveals the lifetime of ^{1}(**9**)* to be ca. 900 ps, in agreement with the longer of the two fluorescence lifetimes. On the basis of these results, we took ca. 900 ps as the lifetime of the relaxed ^{1}(D)*.

In D–M linked models **4–6**, the intramolecular singlet–singlet EN from (M)* to D has been confirmed by fluorescence lifetime measurements. In the fluorescence of **4**, the emission due to M (at 580 nm) decays with τ(M) = 67 ps, while we have observed a fluorescence rise with τ(rise) = 62 ps and a slow decay with τ(decay) = 890 ps at 700 nm where the emitting species is solely D. The observed rise-time constant at 700 nm corresponds quite well to τ(M), indicating the occurrence of a singlet–singlet EN from ^{1}(M)* to D. By using this τ(M) value, we have evaluated k_{EN} with eq 2 to be 1.4 × 10^{10} s^{-1}. The transient absorption

$$k_{EN} = 1/\tau(M) - 1/\tau_0(M) \quad (2)$$

spectra of **4** (Figure 6) also supported the EN from ^{1}(M)* to D. The transient absorption spectrum at 26 ps delay time can be considered as a superposition of the $S_n \leftarrow S_1$ absorptions of D and M. A relatively sharp absorption at 460 nm and bleaching at 540 nm, both of which are characteristic of ^{1}(M)*, disappear within 200 ps. After 200 ps, the time-dependent transient absorption spectra resemble those of ^{1}(**9**)*. k_{EN} was estimated to be 1.2 × 10^{10} s^{-1} by analysis of the decay profile of the transient absorbance at 460 nm. In virtually the same procedure as for **4**, k_{EN} in **5** and **6** have been determined to be 2.0 × 10^{11} and 2.5 × 10^{10} s^{-1}, respectively.

(37) One of the referees commented that a band at 670 nm in the transient absorption spectra of **9** (Figure 5) looks a lot like that of the porphyrin cation. But, we interpret this as being accidental. As described in the text, the fluorescence spectrum of **9** is independent of solvent polarity, suggesting the absence of intradimer CS in ^{1}(D)*. Symmetry-breaking (usually solvent-induced) CS within a symmetric dimer with strong electronic interactions (exciton coupling as in the case of **9**) is quite rare.

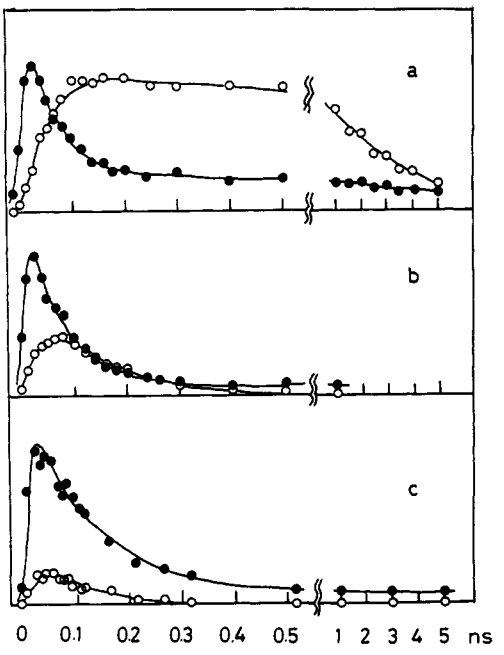

Figure 4. Time profiles in the transient absorption spectra of **7** at 460 nm (●) and at 715 nm (○) in THF and DMF and at 720 nm (○) in (a) C_6H_6, (b) THF, and (c) DMF.

Table I. Electron-Transfer Rate Constant k_{CS} and k_{CR} of **7**

solvent	k_{CS} (s^{-1})[a]	k_{CS} (s^{-1})[b]	k_{CR} (s^{-1})[a]
C_6H_6	1.9 × 10^{10}	1.5 × 10^{10}	3.6 × 10^8
THF	1.7 × 10^{10}	1.3 × 10^{10}	9.3 × 10^9
DMF	0.8 × 10^{10}	0.86 × 10^{10}	~5 × 10^{10}

[a] Determined by the transient absorption spectra. [b] Determined on the basis of the fluorescence lifetime, using the following equation: $k_{CS} = 1/\tau(M) - 1/\tau_0(M)$, where τ(M) is the fluorescence lifetime of **7** and τ_0(M) is the fluorescence lifetime of **8**.

Excited-State Dynamics of 1 in THF. Figure 7b shows the transient absorption spectra of **1** in THF for excitation at 532 nm. It is interesting to note that the prominent absorbance at 715 nm due to $(Im)^-$ persists even at 5-ns delay time. This contrasts with the behavior of **7** in that $(M)^+$–$(Im)^-$ has only ca. a 100-ps lifetime (Figure 3b). We attribute this long-lived absorbance at 715 nm to the formation of a radical-ion-pair state $(D)^+$–M–$(Im)^-$. The absorption at 460 nm decays biexponentially with τ = 35 and 70 ps. The former time constant is assigned to the decay of ^{1}(M)*, since we have confirmed that the fluorescence lifetime of ^{1}(M)* is 35 ps, and the latter can be assigned to the CR reaction of D–$(M)^+$–$(Im)^-$, according to the following analysis of kinetic trace at 715 nm. Namely, the rapid decay of ^{1}(M)* takes place along with an increase of absorption at 715 nm with a rise-time of 35 ps, which in turn decays biexponentially with 70-ps and >10-ns time constants. Therefore, we assign the 70-ps decay to the CR reaction within D–$(M)^+$–$(Im)^-$ and the remarkably slow decay with a more than 10-ns time constant to the CR reaction of $(D)^+$–M–$(Im)^-$. The spectral shape of the transient absorption in the range of 460–550 nm at 100–200-ps delay time is quite reminiscent of the transient absorption spectra of **9** in the same region and indicates an increase in the amount of ^{1}(D)* from 26 ps to 100–200 ps. These facts suggest that ^{1}(M)* in **1** is quenched by both D and Im, giving rise to the formation of ^{1}(D)*–M–Im and of D–$(M)^+$–$(Im)^-$, respectively. In fact, ^{1}(M)* in **1** (τ(M) = 35 ps) is shorter lived in comparison with that in **7** (τ(M)=60 ps) or **4** (τ(M)=80 ps). Moreover, $1/\tau$(M) for **1** is roughly the sum of $1/\tau$(M) for **4** and $1/\tau$(M)

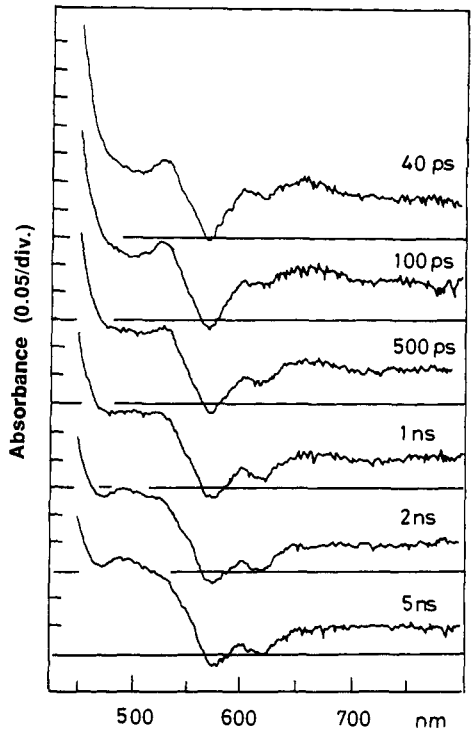

Figure 5. Transient absorption spectra of **9** for excitation at 532 nm in THF.

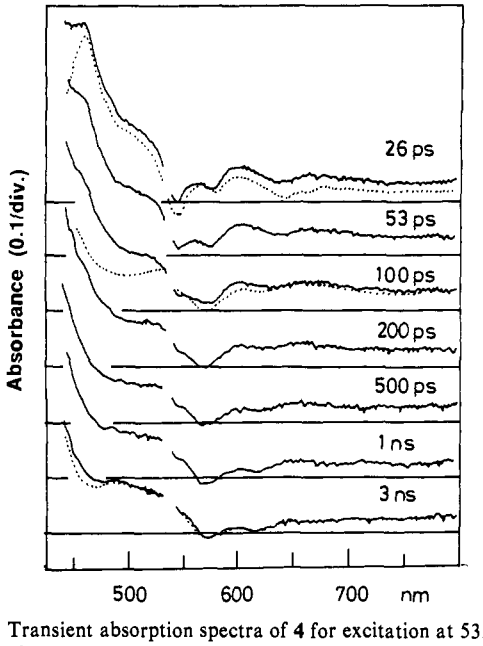

Figure 6. Transient absorption spectra of **4** for excitation at 532 nm in THF. The dotted line at 26-ps delay time indicates the $S_n \leftarrow S_1$ absorption spectrum of **8**, and those at 100 ps and 3 ns indicate the $S_n \leftarrow S_1$ and $T_n \leftarrow T_1$ absorption spectra, respectively, of **9**.

for **7**, which tends to confirm quenching of ^{1}(M)* by both D and Im. On the other hand, the fluorescence lifetime of ^{1}(D)* in **1** is nearly the same as that of **9**, indicating that the ^{1}(D)* is not quenched by either M or Im. This has been confirmed by separate picosecond laser photolysis experiments by exclusively exciting D at 620 nm (Figure 8a), where IP states are virtually undetectable. On the basis of these results, we conclude that long-distance ET from ^{1}(D)* to (Im) does not take place in **1**.

The lifetime (70 ps) of the initially formed IP state D–$(M)^+$–$(Im)^-$ in **1** is distinctly shorter than the lifetime (100 ps) of the $(M)^+$–$(Im)^-$ formed in **7**. This observation indicates the presence of an additional decay channel for the D–$(M)^+$–$(Im)^-$ state other than the CR reaction regenerating the ground-state D–M–Im, since the $(M)^+$–$(Im)^-$ state in **7** decays only by CR. One possible additional decay pathway is hole transfer (HT) from $(M)^+$ to D. Assuming this to be the sole additional decay pathway of D–$(M)^+$–$(Im)^-$, the rate (k_{HT}) of hole transfer in **1** is calculated to be 4.3×10^9 s^{-1} by using eq 3:

$$k_{HT} = 1/\tau_{IP_2} - 1/\tau_{IP_1} \quad (3)$$

where τ_{IP_1} and τ_{IP_2} are the lifetimes of $(M)^+$–$(Im)^-$ and D–$(M)^+$–$(Im)^-$, respectively.

Figure 9 shows the transient absorption spectra of **1** excited at 532 nm in THF in the 0.14–5.5-μs time region. Absorbances at 480, 650, and 715 nm are assigned mainly to ^{3}(D)*, $(D)^+$, and $(Im)^-$, respectively, although ^{3}(D)* has substantial absorption at 650 and 715 nm (see the transient absorption spectrum of **9** at 5-ns delay time in Figure 5) and $(Im)^-$ has substantial absorption at 650 and 715 nm (molar extinction coefficients of $(Im)^-$ have been determined from spectroelectrochemical measurements to be 29 600 at 715 nm and 6400 at 650 nm). Thus, analysis of the decay traces at 480 and 715 nm has revealed the lifetimes of ^{3}(D)*, $(D)^+$, and $(Im)^-$ to be 0.33, 2.5, and 2.5 μs, respectively, under anaerobic conditions. The lifetime of the ^{3}(D)* was significantly reduced to less than 100 ns by addition of oxygen, while the initial amplitudes and lifetimes of $(D)^+$ and $(Im)^-$ were virtually unaffected by oxygen.

On the basis of these kinetic results, the reaction scheme of **1** in THF can be depicted as summarized in Scheme III, where k_1 is $1/\tau_0(M) = 7.4 \times 10^8$ s^{-1}, k_2 is $1/\tau_0(D) = 1.1 \times 10^9$ s^{-1}, k_3 is the CR rate of $(D)^+$–M–$(Im)^-$, k_{CS} and k_{CR} are assumed to be the same as those in **7**, respectively, and k_{EN} is assumed to be the same as that in **4**. It should be noted here that since k_3 is much smaller than the other rate constants, the time dependence of the transient absorbances of **1** in the porphyrin $S_n \leftarrow S_1$ and $(Im)^-$ absorption bands in THF (and also of **2** as well as **3**, as discussed later) seems to be given by the same type of biexponential equation (1), at least in the relatively early stage of several 100 ps. Namely, if we neglect k_3 and also the relatively slow process depicted by k_2, the time profiles of M*(D–^{1}(M)*–Im), D*(^{1}(D)*–M–Im), IP_1(D–$(M)^+$–$(Im)^-$), and IP_2($(D)^+$–M–$(Im)^-$) are given by:

$$[M^*] = A_0 \exp(-t/\tau_M)$$

$$[D^*] = B_0 + A_0 \tau_M k_{EN}\{1-\exp(-t/\tau_M)\}$$

$$[IP_1] = A_0 k_{CS} \tau_M \tau_{IP_1} (\tau_M - \tau_{IP_1})^{-1}\{\exp(-t/\tau_M) - \exp(-t/\tau_{IP_1})\}$$

$$[IP_2] = A_0 k_{CS} k_{HT} \tau_{IP_1} \tau_M (\tau_M - \tau_{IP_1})^{-1}\{(\tau_M - \tau_{IP_1}) + \tau_{IP_1} \exp(-t/\tau_{IP_1}) - \tau_M \exp(-t/\tau_M)\}$$

where A_0 and B_0 are the initial concentrations of M* and D*, respectively, $\tau_M^{-1} = k_1 + k_{CS} + k_{EN}$, and $\tau_{IP_1}^{-1} = k_{CR} + k_{HT}$. From these equations, the time profile at wavelength λ is given by a double-exponential equation of the following form:

$$A_\lambda(t) = a'_\lambda \exp(-t/\tau_M) + b'_\lambda \exp(-t/\tau_{IP_1}) + c'_\lambda \quad (4)$$

If we take k_2 into account, the time profile of D* becomes more complex, although the time profiles of the other species remain the same. In this case, $A_\lambda(t)$ is represented by a three-exponential

$$[D^*] = A_0 k_{EN} \tau_M (1-k_2\tau_M)\{\exp(-k_2 t) - \exp(-t/\tau_M)\} + B_0 \exp(-k_2 t)$$

equation. However, as described above, the observed results of **1** in THF at 460 nm as well as at 715 nm can be reproduced approximately by eq 4 up to the time range of ca. 400–500 ps, owing to the much slower value of k_2 compared with τ_M^{-1} and

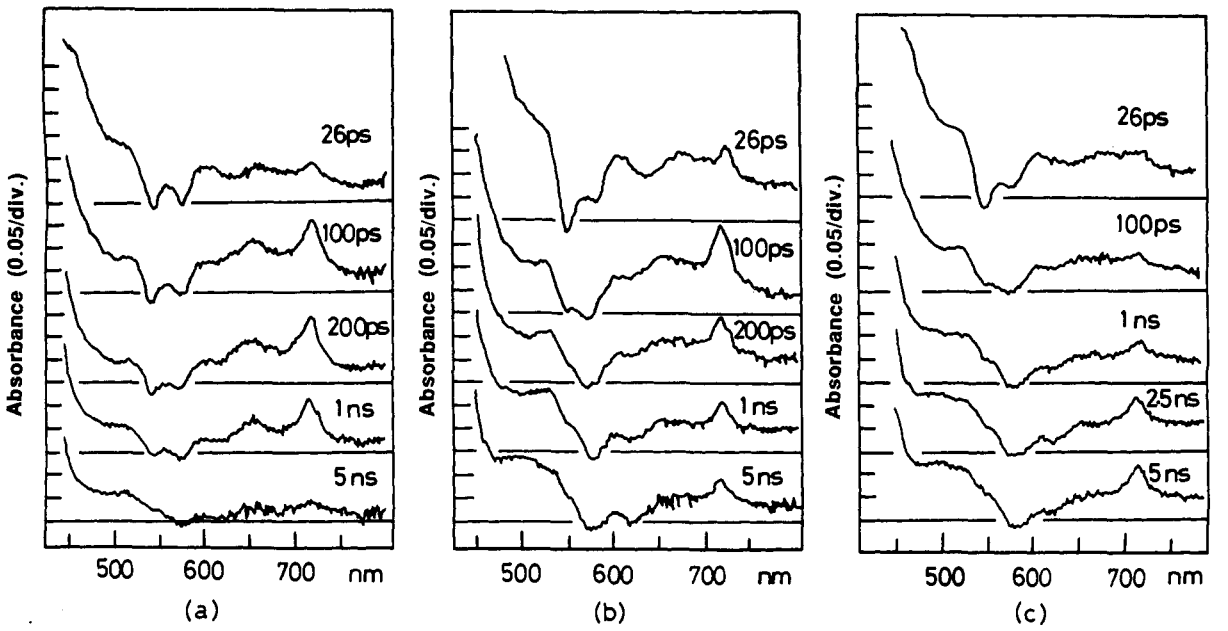

Figure 7. Transient absorption spectra of **1** on a ps–ns time scale for excitation at 532 nm in (a) C_6H_6, (b) THF, and (c) DMF.

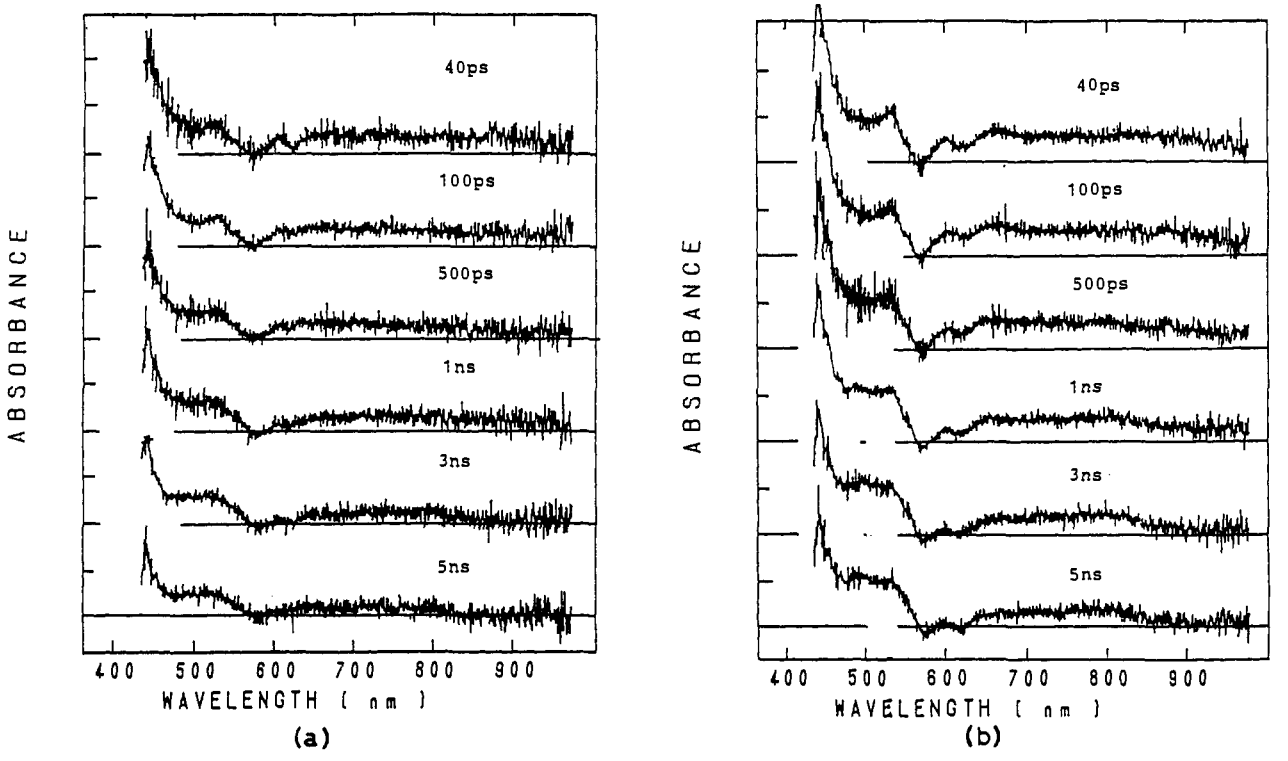

Figure 8. Transient absorption spectra of **1** for excitation at 620 nm in (a) THF and (b) DMF.

$\tau_{IP_1}^{-1}$ values. As discussed in the following section, a similar reaction scheme and time profiles of the transient absorbance appear also to reproduce the observed results obtained for **2** and **3** in THF solutions.

Excited-State Dynamics of 2 and 3 in THF. Excited-state dynamics of **2** and **3** and their acceptor-free models **5** and **6** have also been examined by transient absorption spectroscopy and fluorescence lifetime measurements. Practically the same reaction scheme as written for **1** (Scheme III) can be drawn also for **2** and **3** on the basis of the following facts: (1) the singlet–singlet EN from D–^{1}(M*)–Im to ^{1}(D)*–M–Im is evident in **5** and **6** and therefore in **2** and **3**; (2) the fluorescence lifetimes of ^{1}(M)* in **2** and **3** (main components are 2 ps for **2** and 25 ps for **3**) are much shorter than those in **5** and **6** (main components are 5 ps for **5** and 39 ps for **6**), indicating competitive electron transfer to Im in addition to EN to D; (3) the initially formed IP state D–(M)$^+$–(Im)$^-$ is distinctly shorter lived (35 ps for **2** and 60 ps for **3**) in comparison with the (M)$^+$–(Im)$^-$ state in **7** (100 ps), indicating the presence of hole transfer to produce (D)$^+$–M–(Im)$^-$ besides the CR reaction giving the ground state (the rate of the hole transfer (k_{HT}) has been determined by eq 3 to be 1.9×10^{10} s^{-1} for **2** and 6.7×10^9 s^{-1} for **3**, respectively); (4) long-lived charge-separated IP states with lifetimes of 0.25 and 5.3 μs are indeed formed in **2** and **3**, respectively; and (5) the singlet excited state ^{1}(D)* is not quenched by M or Im in **2** and **3**, and thus ^{1}(D)* does not contribute to formation of the IP state. The kinetic parameters thus calculated are listed in Table II, from which the quantum efficiencies for formation of (D)$^+$–M–(Im)$^-$ from the D–^{1}(M)*–Im state are calculated to be 0.17, 0.05, and 0.16 for **1**, **2**, and **3**, respectively.

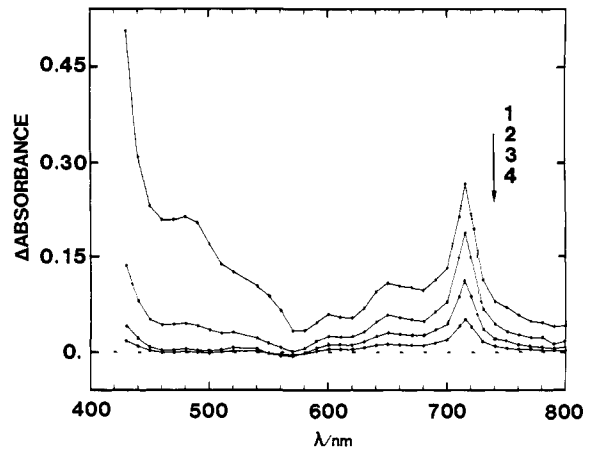

Figure 9. Transient absorption spectra of **1** on a ns–μs time scale for excitation at 532 nm in THF at delay times of (1) 0.14 μs, (2) 0.74 μs, (3) 1.94 μs, and (4) 4.34 μs.

Scheme III. Reaction scheme and energy diagram for **1** in THF

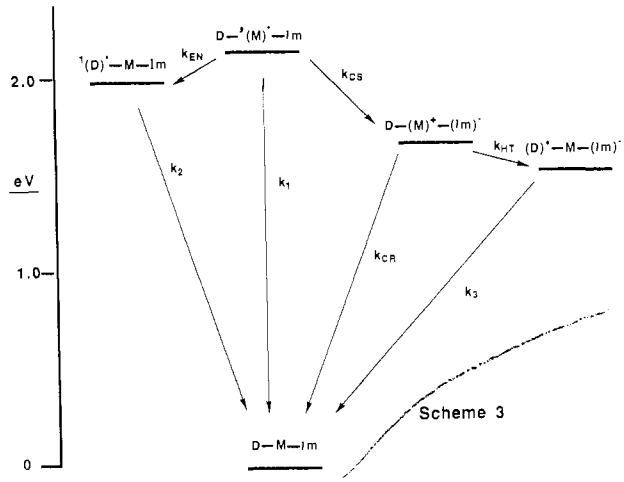

Table II. Kinetic Parameters of Models **1–3** in THF

model	k_{EN}[a] (s^{-1})	k_{HT}[b] (s^{-1})	k_3[c] (s^{-1})	Φ(CT)[d]
1	1.4×10^{10}	4.3×10^{9}	4.0×10^{5}	0.17
2	2.0×10^{11}	1.9×10^{10}	4.0×10^{6}	0.05
3	2.5×10^{10}	6.7×10^{9}	1.9×10^{5}	0.16

[a] Rate of intramolecular singlet–singlet energy transfer from ^{1}(M)* to D determined by eq 2 for the corresponding Im-free models. [b] Rate of hole transfer from (M)$^+$ to D calculated by eq 3. [c] Rate of the CR reaction of (D)$^+$–M–(Im)$^-$. [d] Quantum yield for formation of (D)$^+$–M–(Im)$^-$ from ^{1}(M)*. $\Phi(CT) = k_{CS}(k_{CS} + k_{EN} + k_1)^{-1}k_{HT}(k_{CR} + k_{HT})^{-1}$.

Solvent and Temperature Effects on Excited-State Dynamics. We also examined the excited-state dynamics of **1** in C_6H_6 and in DMF in order to clarify the effect of solvent polarity on the excited-state dynamics of triad **1**. The transient absorption spectra taken in C_6H_6 and DMF are presented in Figures 7a and 7c. The transient absorbance of (Im)$^-$ at 715 nm in **1** decays with a lifetime of 2.5 ns in C_6H_6, which is almost identical with the lifetime (2.8 ns) of (M)$^+$–(Im)$^-$ formed from **7** in the same solvent. These results have led us to conclude that in C_6H_6, the D–(M)$^+$–(Im)$^-$ state decays only by the CR reaction and the hole transfer does not occur. On the other hand, we observed the formation of a long-lived IP state in polar DMF or *n*-butyronitrile solution; the lifetime of the (D)$^+$–M–(Im)$^-$ state has been determined for **1** (8.2 μs), **2** (0.39 μs), and **3** (23 μs) in DMF and for **1** (5.9 μs) and **3** (16 μs) in *n*-butyronitrile. It should be stressed here that an increase of the solvent polarity increases the lifetime of (D)$^+$–M–(Im)$^-$ regardless of the spacer connecting D and M in contrast to the solvent effects found for the CR reaction of (M)$^+$–(Im)$^-$.

Finally, the lifetimes of (D)$^+$–M–(Im)$^-$ in **1** and **3** were measured as a function of temperature in the range of 200–300 K in *n*-butyronitrile. Activation energies of 6.0 and 4.4 meV were obtained for **1** and **3**, respectively. These results indicate that the CR is essentially activationless.

Synthesis. The synthesis of the 1,2-phenylene-bridged diporphyrin **9** was reported elsewhere.[24] The synthetic route to **1–3** and their acceptor-free reference molecules **4–6** is shown in Scheme I. A synthetic method used for the synthesis of oligomeric porphyrins[30] was also employed here. Condensation of the formyl-substituted porphyrin **10**,[24] bis(3-ethyl-4-methyl-2-pyrrolyl)-methane (**11**),[31] and aldehydes **12–14**[32] in the presence of trichloroacetic acid in acetonitrile followed by oxidation with *p*-chloranil and acidic deprotection provided formyl-substituted 1,2-phenylene-bridged diporphyrins **15–17** in 30–50% yields based on the amounts of **10** used. Since 1,2-phenylene-bridged diporphyrins in their free-base form have very low R_f values on silica gel, it was rather easy to separate **15–17** in a pure state from the reaction mixture. Similar condensations of **15–17** and pyromellitimide-linked aldehyde **18** with **11** followed by zinc insertion gave triads **1**, **2**, and **3** in 18, 7, and 32% yields, respectively. Acceptor-free models **4–6** were prepared similarly from the condensations of **15–17** and aldehyde **19** with **11** in 73, 53, and 30% yields, respectively. The reference monomeric model **7** was prepared by the acid-catalyzed condensation reaction of **18** and *p*-tolualdehyde with **11**.[33] All models studied in this paper were fully characterized by 400 MHz ^{1}H-NMR and mass spectral analysis.

Discussion

In D–M and D–M–Im models, the D moiety closely duplicates some aspects of photosynthetic functions of the SP in bacterial RCs acting as an energy sink and an electron donor toward the M moiety. As described above, analyses of photoexcited-state dynamics were remarkably facilitated by monitoring the absorption bands of (Im)$^-$, and we have been able to determine all the rates involved in Scheme III, which are summarized in Table II. We also found that the photoexcited-state dynamics are greatly influenced by polarity of the solvents not only in the rates of electron-transfer reactions but also in the reaction course.

With regard to the function of an energy sink, in the natural RCs, the excitation energy absorbed by photosynthetic pigments is efficiently transferred to the special pair to yield its singlet excited state, from which a stable ion pair state, (SP)$^+$–BChl–(BPh)$^-$, is formed within 3 ps. As characterized by the X-ray structure determinations, two of the BChl molecules are closely associated spatially and electronically to form the special pair (SP).[2,4] The two BChl molecules that comprise the SP have the same chromophore as the other BChl molecules that function as antenna pigments. Extended electronic interactions between the two BChl molecules lead to the unusual chemical and spectroscopic properties of the SP, thus enabling the SP to act as both the final singlet energy sink of the energy-relay system as well as the initial electron donor in the RC. For all of the D–M linked models studied here, an efficient singlet–singlet EN from ^{1}(M)* to D was observed. This process is quite similar to the observed mode of an efficient singlet–singlet EN in the natural RC where the SP is the final energy sink. To the best of our knowledge, this is the first example of unidirectional EN from monomer to dimer comprising the same porphyrin chromophore. In the present models, the ^{1}(D)* lies at a 1.93–1.97-eV energy level, which is lower than that of the ^{1}(M)* by 0.16–0.23 eV, thus precluding reversible EN. Significant spectral overlap of the emission spectra of the donor ^{1}(M)* and the absorption spectra of the acceptor (D) facilitates efficient EN, while spectral overlap of the emission spectra of ^{1}(D)* and the absorption spectra of M

is negligibly small. Faster energy transfer in **3** or **6** compared with **1** or **4** indicates the importance of center-to-center separation rather than the through-bond interactions in singlet–singlet energy transfer, since the center-to-center separation between the D and M in **3** is slightly shorter than that in **1**, but the D and M in **3** have one more methylene group in the bridging spacer than those in **1**. A similar trend was previously observed in a zinc free-base hybrid diporphyrin system.[25,63]

Another important finding is that the D moiety can also function as an effective electron donor to the M moiety, realizing the formation of the long-lived IP states in the triads **1–3**. The lifetimes of such IP states range from 0.25 to 23 μs, depending upon both the spacer connecting the D and M and the polarity of the solvent. On the basis of picosecond transient absorption data, however, it has now been revealed that $(D)^+$–M–$(Im)^-$ is formed from D–$^1(M)^*$–Im via D–$(M)^+$–$(Im)^-$. The reaction course to the final IP state therefore differs from that occurring in the bacterial RCs, since in the natural systems the initial CS between the SP and BPh is followed by electron transfer to Q_A.

Electron-transfer reactions are regulated by a variety of parameters, including the free energy gap (ΔG^0) between the initial and final states; the magnitude of the electronic interaction between the donor (D) and acceptor (A), which is dependent on the mutual distance and orientation as well as on the molecular nature of the bridging group or medium; and the overall reorganization energy (λ) involving both the external (λ_s) and internal reorganization (λ_i).[17,39,40] As solvent polarity increases, IP states are stabilized by interaction with solvent dipoles. It should be noted here that in the case of such large conjugated π-electronic systems as in the compounds used here, λ_i is considerably larger than λ_s in low dipolar solvents like C_6H_6 while λ_s becomes comparable to or larger than λ_i in polar solvents like THF or DMF.[35] In the classical Marcus approach,[41] the barrier $\Delta G^{\ddagger}$ to electron transfer can be expressed by eq 5, where λ denotes the sum of λ_i and λ_s, while the rate constant (k) is given by eq 6, where k_B represents the Boltzmann constant and the preexponential factor A is determined mainly by the degree of electronic coupling.

$$\Delta G^{\ddagger} = (\Delta G^0 + \lambda)^2/4\lambda \quad (5)$$

$$k = A \exp(-\Delta G^{\ddagger}/k_B T) \quad (6)$$

The bell-shaped dependence of the ET rate constant on the energy gap covering both the inverted and normal regions as predicted by conventional theories has been confirmed only recently for the charge-shift reaction in fixed-distance models[42] and for the CR decay of geminate radical-ion pairs produced by fluorescence quenching of nonlinked D and A in polar solutions.[43] In the case of CR in covalently linked D–A pairs, however, no normal region but only the inverted region has been observed so far.[29,35,44] In contrast, no inverted region but only the normal region has been observed in the photoinduced CS reaction for both nonlinked[45,46] and linked D–A pairs.[29,35,47–49] Several theoretical interpretations have been proposed to remedy this apparently contradictory situation.[50]

Table III. Estimated Energy Level (eV) for Models **1** and **7**

	C_6H_6	THF	DMF
$^1(D)^*$	1.97	1.97	1.93
$^1(M)^*$	2.13	2.13	2.16
$(D)^+$–$(M)^-$	2.83	2.20	2.00
$(M)^+$–$(Im)^-$	2.38	1.65	1.43
$(D)^+$–M–$(Im)^-$	2.42	1.49	1.19

[a] Excitation energies of D and M are estimated on the basis of the fluorescence and absorption data. The energies of the ion pair states in DMF were a simple sum of the electrochemical potential of the respective chromophore; the one-electron oxidation potentials of D and M are –0.05 and 0.19 V, and the one-electron reduction potentials of Im and M are –1.24 and –2.05 V vs ferrocene/ferrocenium ion. The energies of the ion pair states in C_6H_6 and THF were estimated by $E(IP) = E_{ox} - E_{red} + \Delta G_s$, $\Delta G_s = (e^2/2)(1/r_D - 1/r_A)(1/4\pi\epsilon_0\epsilon - 1/4\pi\epsilon_0\epsilon_r) - e^2/4\pi\epsilon_0\epsilon R_{DA}$, where E_{ox} and E_{red} are oxidation and reduction potentials of the donor and acceptor, respectively, measured in DMF; r_D and r_A are effective radii of the donor cation and acceptor anion; and ϵ_r and ϵ are dielectric constants of DMF and C_6H_6 or THF, respectively. The radii of $(D)^+$, $(M)^+$, and $(Im)^-$, were taken to be 5, 5, and 3.5 Å, respectively, and the separation (R_{DA}) between charges to be 17.9 Å for $(D)^+$–$(M)^-$, 13 Å for $(M)^+$–$(Im)^-$, and 29.8 Å for $(D)^+$–M–$(Im)^-$, respectively.

The excitation energies of D and M and the estimated energies of IP states such as $(D)^+$–$(M)^-$, $(M)^+$–$(Im)^-$, and $(D)^+$–M–$(Im)^-$ for the models **1** and **7** are listed in Table III. The energies of $^1(D)^*$ and $^1(M)^*$ have been obtained by averaging the energies of the corresponding peaks in the fluorescence and absorption band. The energies of the IP states in DMF were estimated from a simple sum of the one-electron oxidation and reduction potentials of the relevant chromophore in DMF, and those in THF and C_6H_6 were calculated by using the corrected solvation energies with the Born equation.[34] Estimation of IP state energies in low dipolar solvents is risky, and it must be kept in mind that the listed values should be regarded only as a rough estimate. In general, the estimation of the IP energy by the Born equation overestimates the correction term ΔG_s in low dipolar solvents. We believe that the IP states in C_6H_6 should lie at 0.3–0.4 eV lower than the calculated energy levels. It is clear that the actual energy level of $(M)^+$–$(Im)^-$ in C_6H_6 lies lower than the estimated level (2.38 eV) in Table III, since efficient CS in **7** does in fact take place from $^1(M)^*$ which lies at 2.13 eV.

It is evident from Table I that k_{CS} in **7** does not show a large solvent-polarity dependence in contrast to CR which shows a

(38) Only a limited number of models, where interporphyrin ET has been observed, have appeared. See: (a) Netzel, T. L.; Kroger, P.; Chang, C. K.; Fujita, I.; Fajer, J. *Chem. Phys. Lett.* **1979**, *67*, 223. (b) Bucks, R.; Netzel, T. L.; Fujita, I.; Boxer, S. G. *J. Phys. Chem.* **1982**, *86*, 1947. (c) Overfield, R. E.; Scherz, A.; Kaufmann, K. J.; Wasielewski, M. R. *J. Am. Chem. Soc.* **1983**, *105*, 4256. (d) Wasielewski, M. R.; Johnson, D. G.; Niemczyk, M. P.; Gaines, G. L., III; O'Neil, M. P.; Svec, W. A. *J. Am. Chem. Soc.* **1990**, *112*, 6482. (e) Gust, D.; Moore, T. A.; Moore, A. L.; Gao, F.; Luttrull, D.; DeGraziano, J. M.; Ma, X. C.; Makings, L. R.; Lee, S.-J.; Trier, T. T.; Bittersmann, E.; Seely, G. R.; Woodward, S.; Bensasson, R. V.; Rougée, M.; De Schryver, F. C.; Van der Auweraer, M. *J. Am. Chem. Soc.* **1991**, *113*, 3638.

(39) Marcus, R. A.; Sutin, N. *Biochim. Biophys. Acta* **1985**, *811*, 265.

(40) Mataga, N. Femtosecond-Picosecond Laser Photolysis Studies on Electron Transfer Dynamics and Mechanism in Some Model Systems. In *Perspectives in Photosynthesis*; Jortner, J., Pullman, B., Eds.; Kluwer Academic: Dordrecht, 1990; p 227.

(41) (a) Marcus, R. A. *J. Chem. Phys.* **1956**, *24*, 966. (b) Marcus, R. A. *Annu. Rev. Phys. Chem.* **1964**, *15*, 155.

(42) Calcaterra, L. T.; Closs, G. L.; Miller, J. R. *J. Am. Chem. Soc.* **1983**, *105*, 670. Miller, J. R.; Calcaterra, L. T.; Closs, G. L. *Ibid.* **1984**, *106*, 3047. Closs, G. L.; Calcaterra, L. T.; Green, N. J.; Penfield, K. W.; Miller, J. R. *J. Phys. Chem.* **1986**, *90*, 3673.

(43) Observations of both the inverted and normal regions; see: (a) Mataga, N.; Asahi, T.; Kanda, Y.; Okada, T.; Kakitani, T. *Chem. Phys.* **1988**, *127*, 249–261. (b) Ohno, T.; Yoshimura, A.; Mataga, N. *J. Phys. Chem.* **1986**, *90*, 3295. (c) Mataga, N.; Kanda, Y.; Okada, T. *J. Phys. Chem.* **1986**, *90*, 3880. Observations of the inverted region; see: (d) Gould, I. R.; Ege, D.; Mattes, S. L.; Farid, S. *J. Am. Chem. Soc.* **1987**, *109*, 3794.

(44) Irvine, M. P.; Harrison, R. J.; Beddard, G. S.; Leighton, P.; Sanders, J. K. M. *Chem. Phys.* **1986**, *104*, 315–324.

(45) Rehm, D.; Weller, A. *Israel J. Chem.* **1970**, *8*, 259–271.

(46) (a) Mataga, N.; Kanda, Y.; Asahi, T.; Miyasaka, H.; Okada, T.; Kakitani, T. *Chem. Phys.* **1988**, *127*, 239. (b) Nishikawa, S.; Asahi, T.; Okada, T.; Mataga, N.; Kakitani, T. *Chem. Phys. Lett.* **1991**, *185*, 237.

(47) Joran, A. D.; Leland, B. A.; Felker, P. M.; Zewail, A. H.; Hopfield, J. J.; Dervan, P. B. *Nature* **1987**, *327*, 508–511.

(48) Wasielweski, M. R.; Niemczyk, M. P. In *Porphyrin-Excited States and Dynamics*; Gouterman, M., Rentzepis, P. M., Straub, K. D., Eds.; ACS Symposium Series 321, pp 154–165.

(49) Antolovich, M.; Keyte, P. J.; Oliver, A. M.; Paddon-Row, M. N.; Kroon, J.; Verhoeven, J. W.; Jonker, S. A.; Warman, J. M. *J. Phys. Chem.* **1991**, *95*, 1933.

(50) (a) Yoshimori, A.; Kakitani, T.; Enomoto, Y.; Mataga, N. *J. Phys. Chem.* **1989**, *93*, 8316. (b) Kakitani, T.; Yoshimori, A.; Mataga, N. *J. Phys. Chem.* **1992**, *96*, 5385.

large decrease in rate with decreasing solvent polarity. In the CS reaction, both $-\Delta G^0$ and λ_s increase with solvent polarity in qualitative agreement with usual theory, whereas in the CR reaction, $-\Delta G^0$ decreases with solvent polarity but λ does not seem to change so much, i.e., effects of λ_s seem to be smaller for CR (in the inverted region) than for CS (in the normal region).[35] Therefore, k_{CS} is not affected much by an increase or decrease of solvent polarity, while k_{CR} increases with an increase of solvent polarity or decreases with a decrease in solvent polarity. Consequently, the $(M)^+$–$(Im)^-$ state is longer lived in C_6H_6 but somewhat shorter lived in DMF in comparison with THF. The dramatic increase of the lifetime of the IP state upon lowering the medium polarity stresses the importance of a relatively nonpolar environment in slowing down the undesirable CR reaction as well as in maintaining a high concentration of the charge-separated state in a simple 1:1 linked donor–acceptor compound like **7**.[29,44,49,51]

On the other hand, for triad model **1**, formation of the long-lived IP state $(D)^+$–M–$(Im)^-$ is not achieved in C_6H_6. Failure of hole transfer in less polar C_6H_6 solution may be ascribed to a higher energy level of IP state $(D)^+$–M–$(Im)^-$ than that of the initially formed IP state D–$(M)^+$–$(Im)^-$. Conversely, formation of $(D)^+$–M–$(Im)^-$ in THF and DMF suggests that the $(D)^+$–M–$(Im)^-$ state in these solvents lies at lower energies than the D–$(M)^+$–$(Im)^-$ state and the hole-transfer step proceeds with a rate constant comparable to the relatively rapid CR step. In fact, it is quite general that the charge-separated state will become less stabilized with increasing separation of charges due to the loss of electrostatic energy, and this effect should be more important in solvents of low dielectric constant. These considerations seem qualitatively consistent with the estimation in Table III. On the other hand, in polar solvents, hole transfer in D–$(M)^+$–$(Im)^-$ produces $(D)^+$–M–$(Im)^-$. What we learn from these results is that somewhat polar environments are necessary to achieve a long-lived IP state by a consecutive two or more step electron transfer. The k_{HT} value increases in the order of **1** < **3** < **2**. This may reflect the relative magnitude of the electronic matrix element in the hole-transfer reaction. Faster electron transfer in the porphyrin model bridged by the methylenebis(1,4-phenylene) group compared with the model bridged by the 4,4′-biphenylylene group was previously observed for the CS reaction of zinc–ferric hybrid diporphyrin models.[62] This indicates again the importance of center-to-center separation rather than the through-bond interactions in the hole-transfer reaction. This comparison may be interesting in that we may attribute some part of the electronic coupling necessary for ET to through-space interaction in the case of porphyrin pigments held at a center-to-center distance comparable to their diameters.

In contrast to extensive theoretical and experimental efforts devoted to CR of simple $(donor)^+$–$(acceptor)^-$ IP states, much less attention has been focused on CR reaction of $(donor)^+$–$(sensitizer)$–$(acceptor)^+$ type IP states. In their carotenoid–porphyrin–quinone (C–P–Q) triad systems, Gust et al. reported that the CR reaction of $(C)^+$–P–$(Q)^-$ proceeds via two-step electron transfer involving the C–$(P)^+$–$(Q)^-$ species as a real intermediate.[19g] Their conclusion was based on experimental observations that the CR rate is independent of the spacer connecting P and Q but does not depend on the spacer between C and P. A substantial activation energy was observed for the CR process. In our triads, the lifetime of $(D)^+$–M–$(Im)^-$ depends on the spacer between D and M and increases in the order **2** < **1** < **3** in all solvents examined. If endergonic electron transfer from $(D)^+$–M–$(Im)^-$ to D–$(M)^+$–$(Im)^-$ were the rate-determining step in the CR decay of $(D)^+$–M–$(Im)^-$, a substantial activation energy might be expected. This is not the case. Activation energies experimentally determined (viz. 6.0 and 4.4 meV for **1** and **3** in butyronitrile, respectively) indicate that the CR decay of $(D)^+$–M–$(Im)^-$ is virtually activationless. We therefore consider that the CR of $(D)^+$–M–$(Im)^-$ takes place without involvement of D–$(M)^+$–$(Im)^-$ as a real intermediate. We also found that k_3 decreases with an increase of solvent polarity, being opposite to the case of k_{CR} in **7**. An important structural difference in $(M)^+$–$(Im)^-$ and $(D)^+$–M–$(Im)^-$ for the CR decay is the availability of an intervening, energetically lower-lying π-orbital in the latter. Thus, we suggest that in the latter case, superexchange interaction of the $(D)^+$–M–$(Im)^-$ and D–M–Im with involvement of the intervening M π-orbital tends to facilitate the CR reaction. This consideration seems to be consistent with explicit activationless features of k_3 and also with its dependence on solvent polarity, by taking into account a solvent polarity-induced change of an electronic-coupling matrix element.[53]

Recently, superexchange-mediated long-distance electron transfer has attracted considerable interest in interpretation of efficient long-distance ET not only in the natural RC systems[6,54–56] but also in artificial systems.[19h,58] In this connection, Wasielewski et al. have reported the dependence of the CR rate on the lowest unoccupied energy of the intervening spacer in conformationally rigid quinone-linked porphyrins.[59] In conformationally restricted models consisting of free-base porphyrin (H_2P), zinc porphyrin (ZnP), and quinone (Q), Sessler et al. have reported remarkably effective long-distance ET from the distal H_2P to Q.[60,61] They have interpreted such ET in terms of a direct zinc porphyrin-mediated superexchange mechanism.[61] We have also reported similar long-distance ET from the distal H_2P to the acceptor in related models such as H_2P–ZnP–Q and H_2P–ZnP–Im,[25] the structures of which are, with regard to conformational rigidity and the nature of bridging groups, closely related to the present models. Thus we might expect such ET from $^1(D)^*$ to Im in triad models **1**–**3**. However, $^1(D)^*$ in **1** is not quenched by Im even in DMF. The reasons for the inefficiency of long-distance ET from $^1(D)^*$ still remain to be fully explored, but several explanations are possible, such as (1) insufficient electronic coupling between $^1(D)^*$ and Im either directly or indirectly, (2) too low an energy gap, or (3) not a long enough lifetime of $^1(D)^*$ for long-distance ET to occur. The reluctance of $^1(D)^*$ to ET is the main cause for unsatisfactory quantum yields for formation of $(D)^+$–M–$(Im)^-$ in **1**–**3**.

(51) Closs, G. L.; Miller, J. R. *Science* **1988**, *240*, 440.

(52) Osuka, A.; Maruyama, K.; Mataga, N.; Yamazaki, I.; Nishimura, Y. Unpublished results.

(53) The electronic matrix element V_s for superexchange interaction between states i, m, and n, where m is a virtual state, is given by $V_s = V_{mi}V_{nm}/\Delta E_{mi}$,[54] where V_{mi} and V_{nm} are the respective electronic interaction matrix elements between states i and m, and m and n, and ΔE_{mi} is the vertical energy difference between the states i and m. For the CR reaction of $(D)^+$–M–$(Im)^-$, i = $(D)^+$–M–$(Im)^-$, m = D–$(M)^+$–$(Im)^-$, and n = D–M–Im. Since the energy of the $(D)^+$–M–$(Im)^-$ state in DMF solution is lower than that in THF due to the larger stabilization by solvation, ΔE_{mi} will be larger in DMF. This may lead to a smaller k_3 value (Scheme III) in the case of DMF solution. Recently, solvent polarity-induced change of electronic interactions has been reported; see: Liu, J.; Bolton, J. R. *J. Phys. Chem.* **1992**, *96*, 1718.

(54) Plato, M.; Möbius, K.; Michel-Beyerele, M. E.; Bixon, M.; Jortner, J. J. *J. Am. Chem. Soc.* **1988**, *110*, 7279.

(55) Marcus, R. A. *Chem. Phys. Lett.* **1987**, *133*, 471.

(56) Won, Y.; Friesner, R. A. *Proc. Natl. Acad. Sci. U.S.A.* **1987**, *84*, 5511. Won, Y.; Friesner, R. A. *Biochim. Biophys. Acta* **1988**, *935*, 9.

(57) Boxer, S. G.; Goldstein, R. A.; Lockhart, D. J.; Middendorf, T. R.; Takiff, L. *J. Phys. Chem.* **1989**, *93*, 8280.

(58) (a) Johnson, M. D.; Miller, J. R.; Green, N. S.; Closs, G. L. *J. Phys. Chem.* **1989**, *93*, 1173. (b) Heitele, H.; Michel-Beyerle, M. E. *J. Am. Chem. Soc.* **1985**, *107*, 8286. (c) Overing, H.; Verhoeven, J. W.; Paddon-Row, M. N.; Costaris, E.; Hush, N. S. *Chem. Phys. Lett.* **1988**, *143*, 488.

(59) Wasieleweski, M. R.; Niemczyk, M. P.; Johnson, D. G.; Svec, W. A.; Minsek, D. W. *Tetrahedron* **1989**, *45*, 4785.

(60) (a) Sessler, J. L.; Johnson, M. R.; Lin, T.-Y.; Creager, S. E. *J. Am. Chem. Soc.* **1988**, *110*, 3659. (b) Sessler, J. L.; Johnson, M. R.; Lin, T.-Y. *Tetrahedron* **1989**, *45*, 4767. (c) Sessler, J. L.; Johnson, M. R.; Creager, S. E.; Fettinger, J. C.; Ibers, J. A. *J. Am. Chem. Soc.* **1990**, *112*, 9310.

(61) Rodriguez, J.; Kirmaier, C.; Johnson, M. R.; Friesner, R. A.; Holten, D.; Sessler, J. L. *J. Am. Chem. Soc.* **1991**, *113*, 1652.

(62) Osuka, A.; Maruyama, K.; Mataga, N.; Asahi, T.; Yamazaki, I.; Tamai, N. *J. Am. Chem. Soc.* **1990**, *112*, 4958.

(63) Osuka, A.; Maruyama, K.; Yamazaki, I.; Tamai, N. *Chem. Phys. Lett.* **1990**, *165*, 392.

The solvent effects observed here may have some important practical implications for design of artificial systems capable of realizing efficient charge separation. The advantage of effecting ET reactions in nonpolar environments is useful in increasing IP lifetime in a variety of simple 1:1 donor–acceptor models, since weakly exothermic ET can be very rapid and, by contrast, the reverse CR reaction will be very slow, being at a larger energy gap in the inverted region. However, in cases of multichromophoric molecules such as triads **1–3**, a nonpolar environment may destabilize a long-distance IP state owing to lack of a large Coulombic stabilization energy and a (donor 1)$^+$–(donor 2)–(acceptor)$^-$ state can be longer lived in polar environments, as is actually found for **1–3**.

In models **1–3**, the long-lived IP states are indeed formed in THF, BN, or DMF but the quantum yields of their formation are low because competitive EN from ^{1}(M)* to (D) leads to the formation of ^{1}(D)* which does not undergo long-distance ET reaction to Im. This limitation could be overcome either by designing molecules with increased thermodynamic driving force for long-distance ET from ^{1}(D)* to Im or by enhancing the degree of electronic coupling between the donor and acceptor. Alternatively, lowering the energy level of the interporphyrin IP state (D)$^+$–(M)$^-$ should lead to enhanced rates of ET from ^{1}(D)* to M, which would be followed by electron transfer to produce the long-lived IP state. If long-distance ET from ^{1}(D)* to the acceptor or charge separation between ^{1}(D)* and M can be realized in a D–M–acceptor triad model, a closer mimic of the natural RC would be achieved with a much higher quantum yield of the charge-separated IP state functioning mechanistically in the same way as the natural system.

Experimental Section

UV–visible spectra were recorded with a Shimadzu UV-3000 spectrometer and steady-state fluorescence spectra were taken on a Shimadzu RF-502A spectrofluorimeter both at room temperature. Relative fluorescence quantum yields were determined by integrating corrected emission spectra. ^{1}H-NMR spectra were recorded on a JEOL GX-400 spectrometer (operating at 400 MHz), chemical shifts being reported in the δ scale in ppm relative to Me_4Si. Mass spectra were recorded on JEOL DX-300 and HX-110 spectrometers. For porphyrin compounds, the positive-FAB (fast atom bombardment) ionization method was used, accelerating voltage 1.5 or 10 kV, Xe atom as the primary ion source. The FAB matrix was 3-nitrobenzyl alcohol/chloroform.

For synthetic use, acetonitrile was refluxed over and distilled from P_2O_5. *N,N*-Dimethylformamide (DMF) was distilled under reduced pressure and stored over molecular sieves. Butyronitrile (BN, 500 g) was heated to 80 °C and stirred for several hours in the presence of Na_2CO_3 (94 g) and $KMnO_4$ (6 g). The precipitates that formed on heating were removed by filtration, and Na_2CO_3 and $KMnO_4$ were added again. After being heated for several hours, BN was distilled under reduced pressure. Other solvents and reagents were reagent grade. Preparative separations were usually performed by flash column chromatography on silica gel (Merck, Kieselgel 60H, Art. 7736).

Fluorescence lifetimes were measured on 10^{-7} M air-saturated solutions with a picosecond time-correlated single-photon counting system.[64] Picosecond transient absorption spectra were measured on ca. 10^{-4} M nitrogen-bubbled solutions by means of a microcomputer-controlled double-beam picosecond spectrometer with a repetitive, mode-locked Nd^{3+}:YAG laser[65a] or with a picosecond dye laser pumped by the second harmonic of a repetitive mode-locked Nd^{3+}:YAG laser.[65b] The second harmonic of the Nd^{3+}:YAG laser pulse or the 620-nm output of the dye laser was used for excitation. A Q-switched Nd^{3+}:YAG laser (Quantel YG580) with second harmonic output (532 nm, 15-ns pulse duration) of 40 mJ was used for measurements of nanosecond transient absorption spectra. The data-acquisition system has been described elsewhere.[66] Solutions of the triad compounds (ca. 10^{-5} M) were deaerated by bubbling with argon.

The molar absorption coefficient of the Im anion radical was determined by means of a quantitative flow–electrolysis method.[67] A DMF solution containing 0.1 mmol of Im and 0.1 mol of tetraethylammonium perchlorate was deaerated with nitrogen. After electrolysis, the sample solution was transferred into a flow-through cell at 0.2 mL/min.

Synthesis of Models. Preparation of 10. Monoprotected phthalaldehyde (440 mg, 2 mmol), **11** (921 mg, 4 mmol), and *p*-tolualdehyde (240 mg, 2 mmol) were dissolved in dry CH_3CN (60 mL) under a nitrogen atmosphere. To this solution was added trichloroacetic acid (64 mg, 0.2 mmol) in CH_3CN (2 mL) by syringe, and the mixture was stirred for 16 h at room temperature in the dark. *p*-Chloranil (1.4 g, 5.7 mmol) dissolved in THF was added, and stirring was continued for 3 h, after which the solvent was evaporated. The residue was roughly purified on a short alumina column (CH_2Cl_2). After metalation with $Zn(OAc)_2$, zinc porphyrin products were separated by flash column chromatography (silica gel, C_6H_6). The first fraction was zinc 5,15-bis(*p*-methylphenyl)porphyrin and the second was the zinc complex of the cross-condensation porphyrin product. The acetal protecting group was hydrolyzed by being heated in a mixture of CF_3CO_2H (8 mL), 10% H_2SO_4 (2 mL), and CH_2Cl_2 (40 mL). The reaction mixture was poured into water, and the organic layer was washed with water followed by aqueous $NaHCO_3$ and dried over anhydrous Na_2SO_4. After evaporation of the solvent, the porphyrin product was precipitated by addition of methanol, giving the free-base porphyrin **10** (470 mg, 35% yield based on the used amount of **11**).

General Procedure for the Preparation of 15–17. Formyl-substituted porphyrin **10** (370 mg, 0.55 mmol) and aldehyde **13** (440 mg, 2.2 mmol) were dissolved in 12 mL of CH_3CN containing trichloroacetic acid (200 mg, 1.25 mmol). Dipyrromethane **11** (633 mg, 2.75 mmol) dissolved in CH_3CN (10 mL) was added, and the resulting mixture was stirred for 18 h in the dark under nitrogen. *p*-Chloranil (1.15 g, 4.65 mmol) was then added, and the mixture was stirred for an additional 5 h. The reaction mixture was poured into water, acidified with concentrated HCl, and extracted twice with $CHCl_3$. The combined organic extracts were washed with aqueous $NaHCO_3$, dried, and treated with a solution of $Zn(OAc)_2$ in methanol. The resulting mixture was again poured into water and dried. Zinc porphyrin products separated on a silica gel column (CH_2Cl_2) were treated with aqueous HCl solution to give a mixture containing monomeric and dimeric free-base porphyrins, which were separated on silica gel. The monomeric porphyrins were eluted by CH_2Cl_2, and the desired diporphyrin was eluted by a mixture of CH_2Cl_2/MeOH (98/2). The diporphyrin was crystallized from CH_2Cl_2/MeOH to give violet-blue crystals. Hydrolysis of the acetal protecting group (refluxing in a mixture of CH_2Cl_2, CF_3CO_2H, and H_2O) gave the corresponding formyl-substituted diporphyrin **16** in 50% yield based on the used amount of **10** (346 mg, 0.28 mmol). Models **15** and **17** were prepared in analogous fashion using aldehydes **12** and **14**, respectively.

General Procedure for the Preparation of 1–6. To a solution of **16** (100 mg, 0.082 mmol) and trichloroacetic acid (75 mg, 0.57 mmol) in 42 mL of dry CH_3CN was added a C_6H_6 solution (12 mL) of aldehyde **18** (211 mg, 0.57 mmol). Then, dipyrromethane **11** (150 mg, 0.65 mL) dissolved in 3 mL of CH_3CN was added to the above solution, and the resulting mixture was stirred for 18 h in the dark under nitrogen before *p*-chloranil (240 mg, 0.98 mmol) was added. After 18 h, the solvent was removed under reduced pressure and the residue was dissolved in CH_2Cl_2. The organic layer was washed with aqueous $NaHCO_3$, dried over anhydrous Na_2SO_4, and evaporated. The residue was separated by silica gel flash column chromatography (CH_2Cl_2/MeOH = 98/2–96/4). The eluate was treated with $Zn(OAc)_2$ and purified on a silica gel column (C_6H_6) to afford red crystals of **2** (14 mg, 0.006 mmol, 7% based on the used amount of **16**). Models **1** and **3–6** were prepared in an analogous fashion. Physical properties of these compounds are as follows:

1. mp > 300 °C. m/z = 2329 (calcd for $C_{144}H_{142}N_{14}O_4Zn_3$ = 2328.9). ^{1}H NMR (400 MHz, $CDCl_3$): 0.91 (t, 3H, Im-hexyl), 1.28 (m, 6H, Im-hexyl), 1.33 (m, 12H, Et), 1.61 (m, 12H, Et), 1.75 (m, 2H, Im-hexyl), 1.80 (t, 6H, Et), 1.88 (t, 6H, Et), 2.40 (s, 6H, Me), 2.44 (s, 6H, Me), 2.53 (s, 6H, Me), 2.81 (s, 6H, Me), 2.84 (s, 3H, tolyl-Me), 2.91 (s, 6H, Me), 2.95 (s, 6H, Me), 3.52 (m, 8H + 4H, Et), 3.64 (m, 4H, Et), 3.78 (t, 2H, Im-hexyl), 4.04 (q, 4H, Et), 4.13 (q, 4H, Et), 5.28 (s, 2H, methylene), 7.2–8.7 (22H, Ar + Im-Ar), 8.40 (s, 2H, meso-H), 8.41 (s, 2H, meso-H), 10.27 (s, 2H, meso-H).

2. mp > 300 °C. m/z = 2252 (calcd for $C_{138}H_{138}N_{14}O_4Zn_3$ = 2252.9). ^{1}H NMR (400 MHz, $CDCl_3$): 0.91 (t, 3H, Im-hexyl), 1.26 (m, 6H, Im-hexyl), 1.34 (t, 6H, Et), 1.35 (t, 6H, Et), 1.60 (t, 6H, Et), 1.69 (t, 6H, Et), 1.77 (m, 2H, Im-hexyl), 1.82 (t, 6H, Et), 1.94 (t, 6H, Et), 2.37

(64) Yamazaki, I.; Tamai, N.; Kume, H.; Tsuchiya, H.; Oba, K. *Rev. Sci. Instrum.* **1985**, *56*, 1187.
(65) (a) Miyasaka, H.; Masuhara, H.; Mataga, N. *Laser Chem.* **1983**, *1*, 357. (b) Hirata, Y.; Mataga, N. *J. Phys. Chem.* **1991**, *95*, 1640.
(66) Ohno, T.; Yoshimura, A.; Mataga, N. *J. Phys. Chem.* **1990**, *94*, 4871.
(67) Ohno, T.; Nozaki, K.; Haga, M. *Inorg. Chem.* **1992**, *31*, 548.

(s, 6H, Me), 2.45 (s, 6H, Me), 2.51 (s, 3H, tolyl-Me), 2.93 (s, 12H, Me), 3.05 (s, 6H, Me), 3.29 (s, 6H, Me), 3.52 (m, 8H + 4H, Et), 3.71 (m, 4H, Et), 3.77 (t, 2H, Im-hexyl), 4.05 (q, 4H, Et), 4.23 (q, 4H, Et), 5.28 (s, 2H, methylene), 7.1–9.1 (16H, Ar), 8.35 (s, 2H, Im-Ar), 8.42 (s, 2H, meso-H), 8.42 (s, 2H, meso-H), 10.30 (s, 2H, meso-H).

3. mp >300 °C. m/z = 1171, 2342 (calcd for $C_{145}H_{144}N_{14}O_4Zn_3$ = 2342.9). ^{1}H NMR (400 MHz, $CDCl_3$): 0.90 (t, 3H, Im-hexyl), 1.3 (m, 6H, Im-hexyl), 1.32 (m, 12H, Et), 1.58 (t, 6H, Et), 1.59 (t, 6H, Et), 1.69 (m, 2H, Im-hexyl), 3.4–3.7 (m, 16H, Et), 3.71 (t, 2H, Im-hexyl), 4.01 (q, 4H, Et), 4.08 (q, 4H, Et), 4.79 (s, 2H, methylene), 5.21 (s, 2H, Im-methylene), 7.17 (d, 1H, Ar), 7.28 (d, 1H, Ar), 7.37 (d, 1H, Ar), 7.64 (d, 1H, Ar), 7.74 (d, 2H, Ar), 7.83 (d, 1H, Ar), 7.99 (d, 2H, Ar), 8.07 (d, 1H, Ar), 8.08 (d, 2H, Ar), 8.12 (m, 2H, Ar), 8.21 (br, 2H, Im-Ar), 8.27 (d, 2H, Ar), 8.38 (s, 4H, meso-H), 8.45 (d, 1H, Ar), 8.53 (d, 1H, Ar), 8.92 (d, 1H, Ar), 8.99 (d, 1H, Ar), 10.24 (s, 2H, meso-H).

4. mp >300 °C. m/z = 2166 (calcd for $C_{136}H_{136}N_{12}O_2Zn_3$ = 2166.9). ^{1}H NMR (400 MHz, $CDCl_3$): 1.29 (t, 6H, Et), 1.32 (t, 6H, Et), 1.60 (t, 6H, Et), 1.62 (t, 6H, Et), 1.83 (t, 6H, Et), 1.89 (t, 6H, Et), 2.41 (s, 6H, Me), 2.54 (s, 6H, Me), 2.56 (s, 6H, Me), 2.82 (s, 6H, Me), 2.84 (s, 3H, tolyl-Me), 2.91 (s, 6H, Me), 2.95 (s, 6H, Me), 3.50 (m, 8H + 4H, Et), 3.66 (m, 4H, Et), 3.90 (s, 3H, OMe), 3.96 (s, 3H, OMe), 4.07 (m, 4H, Et), 4.14 (m, 4H, Et), 4.36 (s, 2H, methylene), 6.88 (dd, 1H, dimethoxyphenyl-Ar), 6.97 (d, 1H, dimethoxyphenyl-Ar), 7.00 (d, 1H, dimethoxyphenyl-Ar), 7.1–9.0 (20H, Ar), 8.40 (s, 4H, meso-H), 10.29 (s, 2H, meso-H).

5. mp >300 °C. m/z = 1045, 2091 (calcd for $C_{130}H_{132}N_{12}O_2Zn_3$ = 2090.8). ^{1}H NMR (400 MHz, $CDCl_3$): 1.33 (t, 6H, Et), 1.35 (t, 6H, Et), 1.60 (t, 6H, Et), 1.69 (t, 6H, Et), 1.85 (t, 6H, Et), 1.94 (t, 6H, Et), 2.38 (s, 6H, Me), 2.52 (s, 3H, tolyl-Me), 2.57 (s, 6H, Me), 2.93 (s, 12H, Me), 3.05 (s, 6H, Me), 3.30 (s, 6H, Me), 3.55 (m, 8H + 4H, Et), 3.72 (m, 4H, Et), 3.91 (s, 3H, OMe), 3.97 (s, 3H, OMe), 4.08 (q, 4H, Et), 4.24 (q, 4H, Et), 4.37 (s, 2H, methylene), 6.89 (dd, 1H, dimethoxyphenyl-Ar), 6.98 (d, 1H, dimethoxyphenyl-Ar), 7.00 (d, 1H, dimethoxyphenyl-Ar), 7.13 (d, 1H, Ar), 7.21 (d, 1H, Ar), 7.62 (d, 2H, Ar), 7.80 (d, 1H, Ar), 7.81 (d, 1H, Ar), 8.04 (m, 2H, Ar), 8.13 (d, 1H, Ar), 8.14 (d, 1H, Ar), 8.36 (d, 1H, Ar), 8.42 (s, 4H, meso-H), 8.67 (d, 1H, Ar), 8.87 (d, 1H, Ar), 8.97 (m, 2H, Ar), 9.08 (d, 1H, Ar), 10.32 (s, 2H, meso-H).

6. mp = 265–267 °C. m/z = 1089, 2180 (calcd for $C_{137}H_{138}N_{12}O_2Zn_3$ = 2180.9). ^{1}H NMR (400 MHz, $CDCl_3$): 1.30 (t, 6H, Et), 1.31 (t, 6H, Et), 1.58 (t, 12H, Et), 1.78 (t, 6H, Et), 1.83 (t, 6H, Et), 2.39 (s, 6H, Me), 2.42 (s, 6H, Me), 2.51 (s, 6H, Me), 2.58 (s, 3H, tolyl-Me), 2.69 (s, 6H, Me), 2.85 (s, 6H, Me), 2.92 (s, 6H, Me), 3.47 (m, 8H + 4H, Et), 3.61 (m, 4H, Et), 3.78 (s, 3H, OMe), 3.80 (s, 3H, OMe), 4.00 (q, 4H, Et), 4.06 (q, 4H, Et), 4.26 (s, 2H, dimethoxyphenyl-methylene), 4.72 (s, 2H, methylene), 6.76 (dd, 1H, dimethoxyphenyl-Ar), 6.80 (d, 1H, dimethoxyphenyl-Ar), 6.93 (d, 1H, dimethoxyphenyl-Ar), 7.0–8.9 (20H, Ar), 8.38 (s, 4H, meso-H), 10.23 (s, 2H, meso-H).

7. mp >300 °C. m/z = 1018 (calcd for $C_{62}H_{62}N_6O_4Zn$ = 1018.4). ^{1}H NMR (400 MHz, $CDCl_3$): 0.90 (t, 3H, Im-hexyl), 1.34 (m, 6H, Im-hexyl), 1.73 (m, 2H, Im-hexyl), 1.74 (t, 6H, Et), 1.76 (t, 6H, Et), 2.39 (s, 6H, Me), 2.48 (s, 6H, Me), 2.73 (s, 3H, tolyl-Me), 3.76 (t, 2H, Im-hexyl), 3.98 (q, 4H, Et), 4.00 (q, 4H, Et), 7.54 (d, 2H, Ar), 7.75 (d, 2H, Ar), 7.93 (d, 2H, Ar), 8.05 (d, 2H, Ar), 8.38 (s, 2H, Im-Ar), 10.17 (s, 2H, meso-H).

8. mp >300 °C. m/z = 720 (calcd for $C_{46}H_{48}N_4Zn$ = 720.3). ^{1}H NMR (400 MHz, $CDCl_3$): 1.77 (t, 12H, Et), 2.52 (s, 12H, Me), 2.73 (s, 6H, tolyl-Me), 4.01 (q, 8H, Et), 7.54 (d, 4H, Ar), 7.94 (d, 4H, Ar), 10.18 (s, 2H, meso-H).

9. mp >300 °C. m/z = 1336 (calcd for $C_{84}H_{86}N_8Zn_2$ = 1338.6). ^{1}H NMR (400 MHz, $CDCl_3$): 1.29 (t, 12H, Et), 1.53 (t, 12H, Et), 2.30 (s, 12H, Me), 2.79 (s, 6H, tolyl-Me), 2.90 (s, 12H, Me), 3.5 (m, 4H + 8H + 4H, Et), 7.10 (d, 2H, Ar), 7.28 (d, 2H, Ar), 7.76 (d, 2H, Ar), 8.11 (AA′BB′, 2H, 1,2-phenylene-Ar), 8.33 (s, 4H, meso-H), 8.35 (d, 2H, Ar), 8.93 (AA′BB′, 2H, 1,2-phenylene-Ar).

10. mp >300 °C. m/z = 673 (calcd for $C_{46}H_{48}N_4O$ = 672.4). ^{1}H NMR (400 MHz, $CDCl_3$): −2.40 (br, 1H, NH), −2.32 (br, 1H, NH), 1.77 (t, 12H, Et), 2.41 (s, 6H, Me), 2.52 (s, 6H, Me), 2.73 (s, 3H, tolyl-Me), 4.02 (q, 8H, Et), 7.55 (d, 2H, Ar), 7.96 (m, 4H, Ar), 8.16 (d, 2H, Ar), 8.41 (d, 2H, Ar), 9.59 (s, 1H, CHO), 10.18 (s, 2H, meso-H).

15. mp >300 °C. m/z = 1302 (calcd for $C_{90}H_{92}N_8O$ = 1301.7). ^{1}H NMR (400 MHz, $CDCl_3$): −6.32 (br, 2H, NH), −5.75 (br, 2H, NH), 1.29 (t, 6H, Et), 1.29 (t, 6H, Et), 1.50 (t, 12H, Et), 2.34 (s, 6H, Me), 2.36 (s, 6H, Me), 2.77 (s, 3H, tolyl-Me), 2.88 (s, 6H, Me), 2.89 (s, 6H, Me), 3.38 (m, 4H, Et), 3.47 (m, 8H, Et), 3.55 (m, 4H, Et), 7.24 (d, 1H, tolyl-Ar), 7.34 (d, 1H, tolyl-Ar), 7.51 (d, 1H, biphenylylene-Ar), 7.71 (d, 1H, tolyl-Ar), 7.84 (d, 1H, biphenylylene-Ar), 7.20 (d, 1H, biphenylene-Ar), 8.16 (d, 1H, tolyl-Ar), 8.23 (s, 4H, biphenylylene-Ar), 8.24 (m, 2H, 1,2-phenylene-Ar), 8.36 (s, 2H, meso-H), 8.37 (s, 2H, meso-H), 8.48 (d, 1H, biphenylylene-Ar), 8.98 (m, 2H, 1,2-phenylene-Ar), 10.23 (s, 1H, CHO).

16. mp >300 °C. m/z = 1226 (calcd for $C_{84}H_{88}N_8O$ = 1224.7). ^{1}H NMR (400 MHz, $CDCl_3$): −6.3 (br, 2H, NH), −5.8 (br, 2H, NH), 1.28 (t, 6H, Et), 1.29 (t, 6H, Et), 1.49 (t, 6H, Et), 1.50 (t, 6H, Et), 2.26 (s, 6H, Me), 2.33 (s, 6H, Me), 2.79 (s, 3H, tolyl-Me), 2.87 (s, 6H, Me), 2.90 (s, 6H, Me), 3.37 (m, 4H, Et), 3.47 (m, 8H, Et), 3.54 (m, 4H, Et), 7.23 (d, 1H, tolyl-Ar), 7.34 (d, 1H, tolyl-Ar), 7.61 (d, 1H, formylphenyl-Ar), 8.05 (d, 1H, formylphenyl-Ar), 7.71 (d, 1H, tolyl-Ar), 8.17 (m, 2H, 1,2-phenylene-Ar), 8.19 (d, 1H, tolyl-Ar), 8.36 (s, 2H, meso-H), 8.38 (s, 2H, meso-H), 8.47 (d, 1H, formylphenyl-Ar), 8.57 (d, 1H, formylphenyl-Ar), 8.98 (m, 2H, 1,2-phenylene-Ar), 10.45 (s, 1H, CHO).

17. mp = 231–236 °C. m/z = 1316 (calcd for $C_{91}H_{94}N_8O$ = 1315.8). ^{1}H NMR (400 MHz, $CDCl_3$): −6.3 (br, 2H, NH), −5.8 (br, 2H, NH), 1.26 (t, 12H, Et), 1.48 (t, 12H, Et), 2.29 (s, 6H, Me), 2.30 (s, 6H, Me), 2.72 (s, 3H, tolyl-Me), 2.88 (s, 6H, Me), 2.89 (s, 6H, Me), 3.30 (m, 4H, Et), 3.44 (m, 8H, Et), 3.52 (m, 4H, Et), 4.46 (s, 2H, methylene), 7.17 (d, 1H, Ar), 7.27 (d, 1H, Ar), 7.33 (d, 1H, Ar), 7.35 (d, 1H, Ar), 7.58 (d, 1H, Ar), 7.66 (s, 2H, formylphenyl-Ar), 7.75 (d, 1H, Ar), 8.06 (s, 2H, formylphenyl-Ar), 8.16 (d, 1H, Ar), 8.28 (d, 1H, Ar), 8.38 (s, 4H, meso-H), 10.16 (s, 1H, CHO).

Acknowledgment. This work was supported by a Grant-in-Aid for Specially Promoted Research (No. 02102005) from the Ministry of Education, Science and Culture of Japan.